Manuscript

The Atlantic Meridional Overturning Circulation as productivity regulator of the North Atlantic Subtropical Gyre

Nave, S.[1*]; Lebreiro, S.[2]; Michel, E.[3]; Kissel, C.[3]; Figueiredo, M. O.[1]; Guihou, A. [3]; Ferreira, A.[4]; Labeyrie, L.[3]; Alberto, A.[1]

[1] Laboratório Nacional de Energia e Geologia, I.P. (LNEG). Estrada da Portela, Apt. 7586. 2610-999 Amadora, Portugal

[2] Instituto Geológico y Minero de España. Calle Ríos Rosas, 23. 28003 Madrid, Spain

[3] Laboratoire des Sciences du Climat et de l'Environnement. IPSL, CEA/CNRS/UVSQ, Université Paris-Saclay, Avenue de la Terrasse. 91198 Gif-sur-Yvette Cedex. France

[4] British Geological Survey, Environmental Science Centre, Keyworth, Nottingham NG12 5GG, UK

* Corresponding author:
e-mail: silvia.nave@lneg.pt; Telephone: + 351 210 924 600

Abstract

Spatially extensive and intense phytoplankton blooms observed off Iberia, in satellite pictures, are driven by significant nutrient supply by upper ocean vertical mesoscale activity rather than by horizontal advection by coastal upwelling. Productivity of oligotrophic regions is still poorly depicted by discrete instrumental and model data sets. The paleoproductivity reconstructions of these areas represent the mean productivity over long-periods bringing new insights into the total biomass fluxes.

Here we present paleoproductivity records from the oceanic Tore Seamount region, covering the period from 140 to 60 Ka. They show higher nutrient supplies during Termination II, Marine Isotopic Stage (MIS)4, MIS6, and warming transitions of the MIS5 sub-stages. The highest nutrient content (higher productivity) in phase with tracers of bottom-water ventilation (benthic_$\delta^{13}C$, $^{231}Pa/^{230}Th$) establishes a strong linkage with Southern Ocean-sourced Waters variability. Low productivity and ventilation over warm sub-stages of MIS5 respond instead to North Atlantic Deep Water.

Assuming that the Tore Seamount is representative of oligotrophic regions, the glacial-interglacial relationship observed between paleoproductivity and Atlantic Meridional Overturning Circulation strength opens new insights into the importance of estimating the total biomass in these regions. The subtropical gyres might play a considerable role in the carbon cycle over (sub-) glacial-interglacial time scales than thought before.

Keywords: Tore Seamount; Productivity; AMOC; Mesoscale eddies

1. Introduction

Most paleoproductivity reconstructions have mainly focused on upwelling areas due to their unique characteristics as major productive ecosystems, contributing to about 25% of the world's fisheries landings (Jennings et al., 2001). Nevertheless, these regions constitute only a small part of the ocean (roughly 5%). Past estimates for the nutrient-depleted subtropical North Pacific Ocean, typically considered as the ocean's desert, suggest that this extensive region significantly contributes to the carbon sequestered from the surface ocean by the ocean biological carbon pump (Emerson et al., 1997; Sarmiento and Gruber, 2002). If illustrative of other subtropical regions, such as the North Atlantic Subtropical Gyre, these large nutrient-depleted areas may be responsible for up to half of the biological pump of carbon to the deep ocean (Emerson et al., 1997; Oschlies, 2002). Moreover, studies based on the mid-latitude North Atlantic (Gil et al., 2009; Schwab et al., 2012) suggest the importance of offshore (oligotrophic) productivity changes over glacial-interglacial cycles to be addressed. These changes likely account for central mechanisms in the past global carbon cycle (Emerson et al., 1997; Oschlies and Garcon, 1998; Williams and Follows, 1998). It is thus essential to understand the processes behind the organic-carbon export in these oligotrophic areas in order to improve comprehensive earth system models that allow predicting future climate changes more accurately.

The Iberian margin is a key region for paleoceanographic studies (e.g. Shackleton et al., 2000). It is represented by the North Atlantic Eastern Boundary Upwelling System, which has been widely targeted for paleoproductivity reconstructions over different periods based on nearshore cores (e.g., Abrantes, 1991; Cayre et al., 1999; Incarbona et al., 2010; Salgueiro et al., 2010). In contrast, past changes in productivity within the adjacent offshore region have received far little attention and only been studied at low temporal resolution (Lebreiro et al., 1997; Marino et al., 2014; Martins et al. 2017).

Presently, subtropical regions can no longer be considered barren deserts as they account as important productive areas due to mesoscale eddy activity (Dufois et al., 2016; Pelegri et al., 2005; Oschlies and Garcon, 1998). Here, we emphasize the importance of phytoplankton biomass generated by means of sub-mesoscale eddy-driven vertical nutrient fluxes (Lévy, 2003; Dufois et al., 2016), due to upper ocean mesoscale activity (Supplementary Fig. 1) over glacial-interglacial timescales.

We report on a multi-proxy high-resolution study of a sedimentary sequence taken at an open ocean site off Portugal [core MD01-2446; Tore Seamount]. The area is part of the eastern boundary of the North Atlantic Subtropical Gyre. The core site is located about 300 km from the coast within a transitional/oligotrophic setting and is ideally positioned to investigate the role of oceanic primary production in surface waters linked to upper ocean mesoscale activity in comparison to onshore productivity driven by variable upwelling [e.g. Abrantes, 1991; Pailler and Bard, 2002]. The combination of several parameters (reflecting oceanic productivity, bottom water flow speed, surface and deep-water masses properties and terrestrial input) enables us to fully characterize the evolution of offshore conditions at the Iberian margin over the period of 140-60 Ka, where climate was as warm or warmer than today (Kukla et al., 2002) and the response of Atlantic Meridional Overturning Circulation (AMOC) enhanced around the transitions from warm to cold sub-stages (Guihou et al., 2011).

2. Core location and modern hydrographic setting

Core MD01-2446 [39°03'N, 12°37'W] is a Calypso Piston Core, 26.60 m in length, taken within the Pole-Ocean-Pole project in 2001 during the MD123 Geosciences cruise on board the RV

Marion Dufresne. It was retrieved from the eastern external slope rim of the Tore Seamount, a crater-like feature, about 100 km in diameter, that rises ~2800 m above the adjacent basin (Fig. 1). The sediment core was recovered at 3547 m water depth. Its location and depth on the external rim of the seamount guarantees negligible influence from lateral downslope sediment transport from the Iberian continental shelf. The far distance to the coast, enables monitoring the past local (though transitional / oligotrophic) oceanic productivity changes (Behrenfeld et al., 2006).

The Iberian Margin is bathed at the surface by the southward branch of the North Atlantic Drift off Iberia (named Portugal Current) and by the northward Portugal coastal counter-current (Fiúza, 1984; Peliz et al., 2005) (Fig. 1). During spring/summer seasons, Iberian coastal surface waters are sourced in the Eastern North Atlantic Central Water that upwells (forming cold and relatively more nutrient-rich surface waters) due to the influence of the trade winds, typically of the Eastern Boundary Upwelling Systems (Fiúza, 1984). The offshore extent of these upwelled cold waters is about 50 km wide (Fiúza, 1983). Present-day offshore influence of upwelled water-related filaments and plumes, formed in the vicinity of capes, does not usually exceed 150-200 km into the open ocean (Sousa and Bricaud, 1992). In contrast, during the winter season, the poleward slope current, described as a narrow slope trapped flow structure, has a turbulent character with an associated mesoscale eddy field (Oliveira et al., 2004; Peliz et al., 2005). The long-lived anticyclones formed during the separation of a poleward slope current at prominent capes are observed off northern Iberia, extending down to water depths > 1000 meters, migrating off slope and into the deep ocean (Peliz et al., 2005) (Fig. 1*).*

Deep-water circulation in the vicinity of the Tore Seamount is influenced by the lower North Eastern Atlantic Deep Water (NEADW), characterized by high oxygen and low nutrient contents, and the Southern Source Bottom Water with high nutrients and lower oxygen contents (van Aken, 2000). At present, the NEADW is a mixture of the Iceland Scotland Overflow Water (23%), Labrador Sea Water (27%) and (47%) Antarctic Bottom Water (AABW) (van Aken, 2000).

Core MD01-2446 is in the range of the North Atlantic Deep Water (NADW) during interglacials and the Southern sourced Ocean Water (SOW) during glacials, allowing reconstruction of past deep oceanic circulation (Adkins et al. 2005).

3. Methods

3.1 Stable carbon and oxygen Isotopes

Surface and deep water records of carbon and oxygen isotopic composition were based, in our study, on the planktonic foraminifera *G. bulloides* and benthic foraminifera *C. wuellerstorfi)*, respectively. A total number of 186 raw samples (2 cm resolution of sampling interval) were freeze-dried, later washed with distilled water, sieved at 63 and 150 μm, and then dried in paper filters for 48 hours in an oven at 40°C. Specimens of *G. bulloides* were picked from the 250-315 μm fraction and *C. wuellerstorfi* from the fraction greater than 250 μm. The $\delta^{18}O$ and $\delta^{13}C$ of *G. bulloides* (3-4 specimen per analysis) and *C. wuellerstorfi* (1-2 specimens per analysis) were measured at the Laboratoire des Sciences du Climat et de l'Environnement (LSCE) in Gif-sur-Yvette, on a Finnegan DELTA plus XP and GV OPTIMA and IsoPrime mass spectrometers. Data is expressed in ‰ versus Vienna Pee-Dee Belemnite (VPDB). VPDB is defined with respect to NBS19 calcite standard (Coplen, 1988). The mean external reproducibility (1σ) of carbonate standards is ±0.05‰ and ±0.03‰ for $\delta^{18}O$ and $\delta^{13}C$ respectively; measured NBS18 $\delta^{18}O$ is –23.2±0.2‰ VPDB. The pooled standard deviation replicate measurements for the studied period is 0.31 ‰ and 0.26 ‰ for $\delta^{18}O$ and $\delta^{13}C$ respectively for *G. bulloides*, and 0.17 ‰ and 0.24 ‰ for *C. wuellerstorfi*. Oxygen isotope values for *C. wuellerstorfi* were corrected to the ambient seawater equilibrium by 0.64 ‰ (Shackleton and Opdyke, 1973).

Analyses of bulk $\delta^{18}O$ were performed in about 50 mg of crushed sediment, treated with 100% phosphoric acid in a Kiel-carbonate device type and loaded into a Finnigan MAT 251 mass spectrometer at MARUM (University of Bremen, Germany). The precision of the equipment is ±0.07‰ for standard repeated measurements.

3.2 Grain size analyses

A volume of 8-25 cm^3 of sediment sample was freeze-dried. When necessary, sample material was disaggregated in a 0.033 mol sodium hexametaphosphate (Calgon) solution, then washed, and sieved over a 63 μm mesh size. In the <63 μm fraction, organic matter was removed with hydrogen peroxide, excess reagent released in a 60°C warm water bath, and the samples washed with distilled water through diatom ceramic candles. Each sample was then homogenised by stirring and immediately measured in a Micrometrics Sedigraph 5100 at the LNEG laboratory. A set of samples was treated with $C_2H_4O_2$ and $C_2H_7NO_2$ to eliminate carbonates, stirred and re-run in the Sedigraph.

Both bulk (189) and carbonate-free (117) samples were analysed. The error of replicated samples is ±0.12 μm for bulk and ± 0.35 μm for carbonate-free analysis. Statistics were calculated for the grain size distribution interval of 0-63 μm. The data is presented as two parameters: percentage of sortable silt (SS%), i.e. %(10-63 mm)/<63 mm (McCave et al., 1995; McCave and Hall, 2006), and mean carbonate-free <63 μm. We have used mean carbonate-free <63 μm, rather than mean sortable silt ($\overline{SS}$, mean grain size of the carbonate-free non-cohesive

10-63 mm interval) because samples of MD01-2446 contain <12% of %SS. However, Supplementary Fig.3 illustrates a good cross-correlation between %SS and carb-free <63% of R2=0.68, therefore achieving the purpose of tracing strength of bottom currents.

3.3 Magnetic analyses

To reconstruct past changes in the average magnetic grain size, ARM (Anhysteretic Remanent Magnetization), IRM (Isothermal Remanent Magnetization), κ (volume low-field magnetic susceptibility) data and hysteresis parameters have been used.

The low field magnetic susceptibility has been measured on u-channels with a 45-mm diameter MS2-C Bartington coil at LSCE. The data were generated every 2 cm with a resolution close to 4 cm and then normalized by volume to get the volume susceptibility (κ). ARM was also acquired on u-channels using a 50µT DC field with a superimposed 0.1T AF peak field along the axis of the u-channel. The translation speed during acquisition was 1 cm/s to secure the full acquisition of ARM (Brachfeld et al., 2004). The κ_{ARM} parameter was obtained by dividing the value of ARM by that of the DC field. Saturated IRM (SIRM) was then acquired, also along the vertical geographical axis at 1 T using a 2G 1.6 m long pulsed solenoid. The measurements of ARM and IRM were made using cryogenic 755-R 2G magnetometers equipped with high-resolution pick-up coils (Weeks et al., 1993) and placed in the µ-metal shielded room at LSCE. As for κ, the measurements were made every 2 cm with a spatial resolution of about 4 cm.

Both ratios κ_{ARM} / κ and ARM/IRM are used as proxies for magnetic grain size changes as they are smaller (greater) for coarse (fine) populations of magnetic particles (King et al., 1982). The above ratios are only empirically related to the magnetic grain size. Therefore, we also performed magnetic hysteresis measurements using an AGM 2900 from Princeton Measurements Corporation every 5 cm. The hysteresis loops were made between +1 and –1 T. After adjustment of the high field slope, the saturation magnetization (Ms), the remanent saturation magnetization (Mrs), and the coercitive field (Hc) were calculated. The remanent coercitive field (Hcr) was then determined by a remanent curve starting by saturation at 1T followed by a stepwise decreasing field, opposed to the saturating one. The Mr/Ms and Hcr/Hc ratio are both related to the domain-state of the magnetic grains, in turn related to the magnetic grain size. These data, although at slightly lower resolution were used to compare with the continuously acquired κ_{ARM} / κ and ARM/IRM ratios.

3.4 Bulk Geochemistry

The biogenic opal content in each sample was measured at LNEG laboratory following the reduction colorimetric technique by molybdate-blue spectrophotometry (Mortlock and Froelich, 1989). All the samples, standards and blanks were duplicated, and therefore opal data was plotted, for each depth, as average value between sample and replicate. The long-term average of the standard deviation of all the pairs of samples/replicates is ± 0.03 wt%.

The siliceous fraction is prone to dissolution in the North Atlantic, and therefore the determination of biogenic opal in pelagic regions, where typically siliceous productivity is low, is known to be limited (Mortlock and Froelich, 1989). For this reason, we have used an additional (and independent) proxy for productivity – the organic carbon (Corg), allowing for comparison with opal data. Even though dependent on bottom water redox conditions, the Corg record generally shows a positive correlation between surface water productivity and organic carbon accumulation in the sediments (Stein, 1990; Nave et al., 2001; Lebreiro et al., 2006; Romero et al., 2008).

The total carbon content was determined in three replicates of 2 mg of freeze-dried, ground and homogenized bulk sediment sample per level, using CHNS-932 LECO elemental equipment at LNEG laboratory. For each replicate, total carbon was analysed, then organic carbon combusted at 400°C temperature (4 steps of 100°C/h plus 3h at 400°C) and analysed for inorganic carbon content ($CaCO_3$). Organic carbon was calculated, for each level, as the difference between total carbon and inorganic carbon ($CaCO_3$) in weight percentage (wt %).

Sedimentary fluxes of productivity data (opal, organic carbon) were determined by using ^{230}Th normalization as it provides a means to achieve more accurate vertical mass accumulation rates (François et al., 2004). Indeed, vertical mass accumulation rates, when corrected to ^{230}Th normalized flux avoids misinterpretations of sediment mass accumulation rates due to sediment focusing on the seafloor by bottom currents (François et al., 2004). Thus, all productivity data was corrected to ^{230}Th normalized flux (Guihou et al., 2010; Guihou et al., 2011), instead of using the sediment Mass Accumulation Rates.

3.5 X-ray analyses

Bulk sediment samples were freeze dried overnight and hand crushed in an opal mortar. The mineralogical characterization of sediment samples by X-ray diffraction (XRD) was carried out using a Philips PW 1710 powder diffractometer with Bragg-Brentano geometry, equipped with a large anode copper tube and a graphite single crystal monochromator. These assays were performed at the X-ray laboratory installed in the Unit of Mineral Resources and Geophysics of LNEG.

Six elements were selected for X-ray fluorescence (XRF) spectrometry tests due to their relevance in marine sediment records: Ca, Sr, Al, Fe, Ti, K and Ba. Powdered samples (approx. 200 mg) were irradiated using an automated wavelength dispersive spectrometer Philips PW 1400 equipped with a rhodium tube to collect five successive counting (30 sec fixed counting-time) at the diagnosis emission line of each one of these elements (Lα for Ba and Kα for the others) and at the corresponding spectral background using suitable analysing crystals. After subtracting the background from the peak counts, selected counting ratios were calculated: Ca, Sr, Ba vs. Al, and K, Fe, Ti vs. Ca.

Because such quick XRF tests have essentially a semi-quantitative character, comparison with 11 discrete samples that were analyzed by ICP-AES at an external certified laboratory (Aveiro University) allowed to validate the geochemical data obtained at the local X-ray laboratory. For funds reasons, only a limited number of samples (11 samples) and elements (Ba as proxy for productivity) could be analyzed and we chose Al and Ba which yielded average RSD (%) of 2.4 % and 1.7 %, respectively.

4. Chronology

In order to achieve a precise chronological framework to define sub-stages (millennial-scale precision) we compared cores located in a narrow region instead of using a global benthic stack (Lisiecki and Raymo, 2005). Indeed, it has been shown that there might be significant differences in large glacial-interglacial transitions of the benthic $\delta^{18}O$ records of different depth/water masses/ocean basins (Waelbroeck et al., 2011).

Over the period 140-60 ka 4 tie-points have been defined between *G. bulloides* oxygen isotopic records of each core (MD95-2040 and MD01-2446) and the *G. bulloides* oxygen isotopic record of core MD95-2042 (Supplementary Fig. 2). MD95-2040 and MD01-2446 indicate a mean sedimentation rate of 5cm/ka over stage 5.

At present, and likely during the time span of the record, the Tore Seamount location is within the same water masses as core MD95-2042, which has a well-established and precise chronology. Thus, we have used the revisited MD95-2042 age model (Govin et al., 2014) based on the AICC2012 ice core chronology (Bazin et al., 2013; Veres et al., 2013), as the reference to build the MD01-2446 chronology, by direct relationship between the planktonic $\delta^{18}O$ records of both cores. Ages between the age control points were calculated by linear interpolation using Analyseries software (Paillard et al., 1996). Errors for the current correlation range between 0.5 to 1.5 ka on the age scale. Assuming that rapid transitions are synchronous, the error is smaller near rapid transitions (and the tie-points) and larger in between.

5. Results

Results of the analysed core, MD01-2446, are presented in comparison with previously published data of coastal sites (cores MD95-2040: 40°34.91'N, 9°51.67'W, 2465 m water depth and MD95-2042: 37°47.99'N, 10°9.99'W, 3146 m) and a nearby offshore core (D11957: 39°03'N, 12°35'W, 3585 m water depth) (table 1).

Core	Reference	Data
MD01-2446	This study	Planktonic $\delta^{18}O$ (*G. bulloides*) Benthic $\delta^{13}C$ (*C. wuellerstorfi*) Benthic $\delta^{18}O$ (*C. wuellerstorfi*) Paleomagnetic data: ARM/IRM, κARM/κ and Mr/Ms SS% and mean carbonate-free <63 μm. $\delta^{18}O$ Bulk sediment Opal content (weight %) Organic carbon (weight %) $CaCO_3$ (weight %)
	Guihou et al., 2010	$^{231}Pa/^{230}Th$
MD95-2042	Cayre et al., 1999	SST °C (summer) based on foraminifera MAT Transfer Function $\delta^{18}O$ (*G. bulloides*)
	Shackleton et al., 2000	Benthic $\delta^{18}O$ (*Globobulimina affinis*, *C. wuellerstorfi, Uvigerina* spp.) Benthic $\delta^{13}C$ (*Globobulimina affinis*, *C. wuellerstorfi, Uvigerina* spp)
	Salgueiro et al., 2010	Export Production ($gC.m^{-2}.yr^{-1}$)
MD95-2040	Abreu et al., 2003	SST °C (summer) based on foraminifera Simmax.28 Transfer Function $\delta^{18}O$ (*G. bulloides)*
D11957	Lebreiro et al., 1997	Primary Productivity (SIMMAX.28 Transfer Function) Polar (SIMMAX.28 Transfer Function) Gyre Margin (SIMMAX.28 Transfer Function) Upwelling (FA20 Transfer Function)

5.1 Coastal versus offshore surface water masses

Comparison between nearshore and offshore areas of the Iberian margin (table 1) was based on changes in $\delta^{18}O$ of planktonic foraminifer *G. bulloides* (Fig. 2A). Over the 140-60 ka interval, oxygen isotopic values from core MD01-2446 vary approximately between 1 and 3 ‰. Typical glacial-interglacial isotopic changes are well recorded with heavier $\delta^{18}O$ values at MIS 6 and 4 and the onset of MIS 5a, and lighter values standing equally for 5e, 5c, and relatively heavier for 5a (Fig. 2A).

During warm phases (well-marked during 5e) isotopic values are heavier offshore (D11957) than nearshore (MD95-2040 and MD95-2042) (Fig. 2A). Oxygen isotopic differences between sites (north-south and east-west) are nearly negligible during glacial MIS 4, and sub-glacial stages 5b and 5d (Fig. 2A).

Sea Surface Temperatures (SST) based on foraminifera (table 1) show warmer temperatures offshore (D11957) than at the northern nearshore site MD95-2040 and more similar to the southern nearshore site MD95-2042 (Fig. 2B).

5.2 Deep water masses

The benthic oxygen isotopic record (δ^{18}O *C. wuellerstorfi*) from core MD01-2446 varies between 3 and 5 ‰ over the studied time interval showing the typical glacial-interglacial variability (Fig. 2C). Compared to the previously published MD95-2042 benthic δ^{18}O record (table 1), values are very similar along MIS 5, but with marked lighter values during MIS 6 (Fig. 2C).

The comparison of benthic δ^{13}C (an indirect indicator of deep-water ventilation; Curry and Oppo, 2005) between MD01-2446 and nearshore core MD95-2042, points to heavier δ^{13}C values (nutrient depleted) offshore, except during the short-time intervals: 106-101 ka and 83-77 ka (Fig. 2D). This observation is reinforced by the similarity of the benthic δ^{13}C with the ^{231}Pa/^{230}Th record, a proxy for AMOC export variability (Guihou et al., 2010), both obtained from core MD01-2446 (Fig. 3A-C, table 1).

The ARM/IRM, κARM /κ, and Mrs/Ms ratios, used to reconstruct past changes in the average magnetic grain size, indicate relatively coarser magnetic grains coincident with periods of depleted δ^{13}C at MD01-2446 (Fig. 3D). The SS% and mean carb-free <63 μm, proxies for sorting and speed of bottom water (Supplementary Fig.3), show an enhanced and well-sorted deep current during MIS 6, MIS 4 and MIS 5b, but slower flow during MIS 5d and 5a and intermediate MIS 5e (Fig. 3E).

5.3 Continental Input

Oxygen isotope ratios of bulk carbonate have been used as an efficient proxy for land transported detrital carbonate to the seafloor during periods of low sea-level stands (Lebreiro et al., 2009). Bulk oxygen isotopes of MD01-2446 show a long term trend toward heavier values through MIS 5 consistent with the relative sea-level curve (Waelbroeck et al., 2002), although the sub-stages of MIS 5 are not clearly defined (Figs. 4A and B).

5.4 Paleoproductivity records

Paleoproductivity variations were estimated using several independent proxies like biogenic opal content, δ^{13}C difference $_{(G.\ bulloides\text{-}C.\ wuellerstorfi)}$ and organic carbon (Corg) (Fig. 5A-D).

The opal content (%) from core MD01-2446 follows a glacial-interglacial and sub-millennial (transitions in sub-stages) variability showing highest siliceous primary productivity mainly during cold periods, MIS4 and 6, and during transitions 5d to 5c and 5b to 5a (Fig. 5A). However, in order to avoid biased interpretations of the opal % record, commonly associated with sediment focusing, the ^{230}Th-normalised opal fluxes (hereafter referred as opal flux) was also used. The opal flux undergoes a similar trend as the opal content (wt %), with larger differences at MIS4 where despite the increased opal %, enhancement of opal flux is not observed (Fig. 5A-B).

The difference between δ^{13}C recorded in planktonic and benthic foraminifera has been long used as a useful indicator of deep ocean carbon storage, and its variations may be explained by changes in the relative strength of export production (Broecker, 1982b; Shackleton et al., 1983; Olivier et al., 2010). δ^{13}C difference $_{\text{(planktonic-benthic)}}$ from MD01-2446, presents general similar trend to opal % record (higher values during MIS4 and 6, and during 5d to 5c and 5b to 5a transitions, Fig. 5C). Moreover, the organic carbon variability is also generally consistent with the opal content, however, with higher variability, mainly from 5b to MIS4 period (Fig. 5A-B).

Log(Ca/Ti) which reflect relative changes of biogenic carbonate and detrital sediment (Hodell et al., 2015) resembles $CaCO_3$ flux (Fig. 5D) presenting an inverse trend in comparison to paleoproductivity proxies (Opal, Corg and δ^{13}C difference $_{\text{(planktonic-benthic)}}$).

The correlation between productivity and δ^{13}C was assessed by statistical analysis. The ^{230}Th-normalized opal is not available for the last δ^{13}C negative anomaly (MIS6, Fig. 3, Fig. 5), since bulk flux was not determined down the 621 cm core depth (age model ≥128 ka). For this reason, the correlation between opal (wt%) and δ^{13}C was used (Supplementary Fig.4), after confirming that the correlation between opal and opal flux are statistically significant (Supplementary Fig.5).

The relationship between opal (wt%) and δ^{13}C (Supplementary Fig.4), estimated through the Pearson correlation coefficient r for 152 samples, is moderate negative ($r = -0.52$) and statistically significant (with a p-value clearly below a significance level of $\alpha = 0.001$). This negative correlation confirms higher productivity coeval lower δ^{13}C values (i.e., coeval with stronger influence of southern ocean waters).

The relationship between opal (wt%) and 230Th-normalised opal flux (Supplementary Fig.5), estimated through the Pearson correlation coefficient r for 144 samples, is moderate positive ($r = 0.55$) and statistically significant (with a p-value clearly below a significance level of $\alpha = 0.001$). Thus, mean to high values of 230Th-normalised Opal flux are expected to coincide with the last observed δ^{13}C negative anomaly (MIS6, Fig. 3, Fig. 5).

Note that opal and δ^{13}C were generally analysed in different support samples (odd and even cm depths respectively), coinciding for nine depth-samples only; this number of samples is generally not enough to measure the strength of a relationship, namely a trustful value for the Pearson correlation coefficient. The remaining opal values used to assess the relationship between opal and $\delta^{13}C$ (152-9 = 143) have been estimated, with each value corresponding to the opal average of the previous and the following cm-samples. This is likely to cause an underestimation of the actual Pearson correlation coefficient.

6. Discussion

6.1 Open ocean versus nearshore hydrographic conditions off Iberia

According to modern conditions in the North Atlantic, the classic temperature gradients of latitudinal sea surface migrate North-South, on a seasonal basis, and tilt NE-SW during summer and autumn (Supplementary. Fig. 4). This is reflected by summer SSTs that indicate similar temperatures in core MD95-2042 and MD01-2446 (Supplementary Fig. 6). By contrast, during winters, there is an increase in temperature gradients along an N-S transect but in absence of upwelling no E-W, i.e. nearshore-offshore, strong temperature gradient occurs (Supplementary Fig. 6).

The $\delta^{18}O$ *G. bulloides* record (Fig. 2A) is more representative of the spring conditions as this is the dominant species during spring in this area (Lombard et al., 2011). In modern spring, the temperature and salinity differences between sites MD01-2446 and MD95-2040 have opposite effects on the calcite $\delta^{18}O$ (Supplementary Fig. 6). Since $\delta^{18}O$ *G. bulloides* is similar at both sites during most of the stage 5, it indicates that similar temperature and salinity gradients have prevailed on the long-term. On a shorter time-scale, the nearshore record (MD95-2040) indicates higher oxygen isotopic values than the offshore record at the end of 5c, 5d-5c, and 5b-5a transitions. This could be due to the transient southward migration of the polar front system, before it reaches a position south of the three sites during stage 5b and 4. This assumption is supported by the highest summer surface temperature, at southern cores, during those periods. Even though the Tore Seamount location is currently a subtropical region, the presence of polar (foraminifera) fauna during glacial stages 4 and 6 and during the 85 ka cold MIS 5b sub-stage (Fig. 6E) also confirms that this area is episodically part of the subpolar region (Lebreiro et al., 1997; Cayre et al., 1999; Abreu et al., 2003) due to the southward migration of the polar frontal system. During most of stage 5e the nearshore record of core MD95-2040 exhibits lighter oxygen isotopic values than offshore MD01-2446 record, while summer SSTs are still lower nearshore than offshore. Unless a large change in seasonal temperature evolution had occurred, this particular trend may result from a salinity decrease at the nearshore site. This could be related to the increased annual precipitation at NW Iberian and its possible influence on the shelf area by river runoff (Sánchez Goñi et al., 2005).

The oxygen isotopic planktonic difference between the south nearshore MD95-2042 site and offshore site during sub-stage 5e, as well 5c and 5a (Fig. 2B), is larger than expected from the present spring temperature and salinity differences between the two sites (Supplementary Fig. 7). It implies therefore a larger winter and spring temperature gradient between the two sites, potentially corresponding to a northward placement of the Azores front compared to its modern spring position.

Concerning the deep-ocean, grain size trends are the result of sediment transport and deposition processes. At depth, variations of the grain size in the sortable silt range have been used to infer the dynamic of near-bottom paleo-current strength (McCave et al., 1995; Bianchi et al., 1999; Hall and McCave, 2000; McCave and Hall, 2006; McCave et al., 2017).

We observe a trend of higher mean carbonate-free <63 μm grain size and %SS in MD01-2446 indicating stronger deep water currents during MIS 6 and 4 and sub-stadial 5b, together with early interstadial 5e (Fig. 3E). Hall and McCave (2000) reported high sortable silt ($\overline{SS}$) at ~2465 m in MD95-2040 on the Portuguese margin during warmer substages of MIS 5, as a result of faster southern flow of the NEADW paleo-current. The apparently opposed dominant speed during glacials in MD01-2446 can only be explained if the grain size parameters are recording a northward bottom (~3500 m) flow at the Tore slope, which we link with AABW (Adkins et al., 2005). This scenario is coherent with the observed variation of depleted $\delta^{13}C$ benthic traces of the AABW (Fig. 3A, E).

On the other hand, the magnetic grain size parameters suggest efficient transport of detrital magnetite by bottom-water flow (corresponding to coarser magnetic grains) during periods of low benthic $\delta^{13}C$ (mainly MIS4 and MIS6, but also at warming transition 5d-c) (Figs. 3A-D). As it has been widely reported for the North Atlantic, NADW production was weaker and slower during these periods, (e.g. Michel et al., 1995; Shackleton et al., 2000; Kissel, 2005) despite increased production above 2000 m depth of Glacial North Atlantic intermediate waters (Michel et al., 1995; Shackleton et al., 2000; Guihou et al., 2011). As a result, the magnetic data appear to selectively illustrate (sub)orbital variability associated with a southern bottom-water at 3500 mwd in the Eastern Atlantic Margin, seen at MD01-2446. The volcanic Canary Islands and/or Cape Verde Islands might be the source of these magnetic grains, commonly Fe-Ti in oxides and silicates.

Channell et al. (2013) report bacterial magnetite on two cores onshore at the SW Iberian margin (MD01-2443 and MD01-2444) varying on stadial-interstadial timescales, similarly to our data. The detrital/biogenic magnetite ratio increased with hematite concentration together with coarser magnetites during stadials and glacial isotopic stages. However, the cores from Channell et al. (2013) are located at the Iberian margin at 2600-2900 m water depth, where a lot of detrital carbonate could have originated from the continental margin (Lebreiro et al., 2009) whereas core MD01-2446, is a deeper core (3547 water depth) and out of Iberian margin influence at is deeper.

Another hypothesis supporting the magnetic signal of this region was recently raised by Yamazaki and Ikehara (2012), in which the resemblance of the pattern of the SUSAS stack in the subtropical Atlantic with dust records from Antarctic ice cores (Schmieder et al., 2000), would be explained by the redistribution to the subtropical Atlantic of biogenic magnetites produced in circum-Antarctic Ocean sediments under iron fertilization by bottom water currents (Yamazaki and Ikehara, 2012).

Whatever is the source of the magnetite particles, the two grain-size data sets converge if the mineralogical components of coarse magnetic size are contained in the silt grain size fractions, transported a long way, northward by bottom currents.

Taking into account the multi proxy approach presented in our study, our preferred interpretation is that the coarse magnetic grain size at site MD01-2446 likely records the northward SOW bottom current during colder periods (more SOW influence at these latitudes) also coinciding with periods of lighter $\delta^{13}C$ (less contribution of NADW) and lower $^{231}Pa/^{230}Th$ values. In fact, our record reveals that warmer periods of weaker influence of SOW correspond to southward intensification of NEADW.

In any case, further investigations are needed to test the potential of magnetic grain size as a proxy for northwards SOW deep current in the Eastern North Atlantic as far from the coast as the Tore Seamount.

6.2 Source of nutrients sustaining paleoproductivity in oligotrophic areas

A paleoproductivity signal consistent with glacial-interglacial climate variability is observed at orbital timescales in the Tore Seamount region. The main question to be addressed is the origin of the nutrients supporting this oceanic productivity.

Given the geographic location and water depth (about 3500 m) of the studied core, we do not expect any contribution from sediments transported across the Tagus abyssal plain upslope to the Tore Seamount by bottom currents (Fig. 1).

Two main alternative sources are therefore possible: 1) sinking material from coastal advection by means of offshore extension of filaments associated with coastal upwelling, similarly to observed in nearby southward regions (Arístegui et al., 2004), and 2) local offshore productivity generated by mesoscale eddy activity at the North Atlantic subtropical gyre. The relative changes in the contribution of both sources may also constitute an additional and possible scenario.

Lighter $\delta^{18}O$ values of bulk sediment in the nearshore Iberian margin, core MD03-2698 (Lebreiro et al., 2009), are associated with enhanced continental carbonate input during periods of low sea-level (colder periods). These inputs should also imply a greater nutrient transport from continental-sourced material (Broecker, 1982; Filippelli et al., 2007) by lateral advection of surface waters to the ocean realm. Interestingly, the offshore bulk $\delta^{18}O$ copies the planktonic foraminifera $\delta^{18}O$ with lighter values during warm periods (Fig. 4), opposed to coastal core MD03-2698 (Lebreiro et al., 2009). This suggests that the bulk $\delta^{18}O$ is a proxy limited to continental input at nearshore regions, and that the Tore Seamount record is out of major continental influence.

Enhanced diatom production in regions such as the tropical Atlantic, has been attributed to be driven by enhanced wind-driven upwelling or density-driven vertical mixing, or by elevated thermocline concentrations of silicic acid supplied to the surface at a constant rate (e.g Bradtmiller et al. 2016; Hendry et al., 2016).

The location of core MD01-2446 is beyond the 50 km extension of coastal upwelling influence (Fiúza, 1983), where current seasonal filaments rarely extends 150-200 km offshore (Sousa and Bricaud, 1992). Considering that during cold phases of MIS5 and during MIS4 and MIS6 the sea level was lower than today (-40m during cold phases of MIS5, and about -80 and -120 during MIS4 and MIS6, respectively), the seasonal filaments, during the low stand sea level, would reach further offshore than present scenario. Considering the position of the isobath of -120 m, the filaments could reach about 30 km further offshore but, still, that would put the site out of the reach of the filaments. Although it has been suggested that filament activity is likely intensified by stronger trade winds during cold glacial periods (Lebreiro et al., 1997), considering a far reaching of 200 km offshore, with a low stand of -120m of sea level, their contribution to the studied site would not be significant. It therefore does not support, by itself, the overall offshore productivity.

Consequently, to explain the overall productivity at the offshore site we propose local sources of nutrients generated by the upper ocean mesoscale eddy activity (Dufois, F. et al., 2016; Lévy, 2003) (Supplementary Fig. 1). This is consistent with the growing body of evidences accumulated over the last decade pointing towards a significant primary productivity in oligotrophic areas (McGillicuddy et al., 1998; Oschlies and Garcon, 1998; Williams and Follows, 1998; Oschlies, 2002; McGillicuddy et al., 2007; Incarbona et al., 2010; Williams, 2011).

Though mesoscale eddies have been shown to be sites of higher nutrient levels and/or biological productivity in the mixed layer compared with the surrounding waters in the ocean. Our multiproxy study, integrating time and space, is a strong evidence that oceanic paleoproductivity variation (likely related to sub-mesoscale driven vertical nutrient fluxes) echoes that of glacial-interglacial climate variability, in strong agreement particularly with the benthic $\delta^{13}C$ and $^{231}Pa/^{230}Th$ records (Fig. 5A,C).

The higher contribution of nutrient-rich AAIW type southern sourced waters and the state of a deeper upper mixed layer during cold periods would enrich the nutrient supply to the photic zone favouring enhanced productivity in the Tore Seamount region.

As recently documented, biogenic opal export at low-latitudes is likely to rely on silicate from the underlying thermocline, the concentration of which is related with the circulation of the ocean interior (Meckler et al., 2013). A pronounced opal maxima during each glacial termination over the past 550,000 years was reported off northwest Africa (Meckler et al., 2013), during the times of a consistent strong deglacial reduction in the formation of silicate-poor glacial North Atlantic intermediate water (GNAIW). Even though Meckler et al. (2013) focus on a coastal upwelling system, where productivity is dependent of nutrients reaching the surface due to upwelled waters related to trade winds intensification, the concentration of silicate at ocean interior would be favourable to increased productivity also at oligothrophic regions if sub-mesoscale driven vertical nutrient fluxes occur. This enhanced productivity, at glacial terminations, was documented reaching latitudes at the Iberian margin, northwards of Tore Seamount position, as evidenced by the diatom and barium records from core MD95-2039 (Thomson et al., 2000).

Enhanced northward advection of AAIW during periods of reduced North Atlantic overturning circulation has also been recently documented (Rickaby and Elderfield, 2005; Pahnke et al., 2008). Increased nutrient supply via intermediate water masses feeding into the thermocline has been suggested to explain the observed opal changes in the E-Atlantic (Meckler et al., 2013), which are consistent with Si isotope distribution patterns from several Atlantic sediment cores (Hendry et al., 2016).

In parallel, our data reveals that at the eastern North Atlantic, periods of weakened North Atlantic Deep Water formation (lighter benthic $\delta^{13}C$) are coeval with higher productivity, suggesting a close relationship between oceanic productivity and resumption of southern ocean waters (Fig. 5; Supplementary Fig.4).

This relationship was previously suggested through simulations with a coupled climate-ecosystem model of intermediate complexity, revealing that during periods of abrupt climatic changes (at millennial timescales), global ocean productivity is sensitive to changes in the Atlantic Meridional Overturning Circulation (Schmittner, 2005).

In the context of our dataset, the coupling between $\delta^{13}C$ and productivity records could be compromised by a circular issue effect, given that the $\delta^{13}C$ spreading of dissolved inorganic carbon is primarily dependent on the interaction of biological uptake at the sea surface. However, as confirmed for the Canary Islands region, the benthic foraminifera mean $\delta^{13}C$ values of *C. wuellerstorfi* are not influenced by sustained high organic matter fluxes, validating this species as a reliable recorder of bottom water $\delta^{13}C$ (Eberwein and Mackensen, 2006). It can thus be assumed a factual affiliation between oceanic productivity changes and AMOC.

We therefore suggest that besides the upwelling intensity, the presence of southern sourced silica-rich waters play a major role on the low-latitude biological productivity record as an important source of nutrients. The deep NADW is slightly reduced during cold sub-stages of MIS 5 but the intermediate water formation (down to 2000 m depth) is greatly enhanced during cold sub-stages (Guihou et al., 2011).

6.3 The 85 ka and 105 ka productivity-events: oceanic nutrient supply

The benthic $\delta^{13}C$ record show lower values during millennial warming transitions 5d to 5c, and to a lesser extent 5b to 5a (Fig. 3A). These nutrient enriched periods are mostly coeval with higher $^{231}Pa/^{230}Th$ values illustrating weakening of the AMOC export at MIS 5d to 5c and at MIS 5b to 5a transitions (Guihou et al., 2010; Guihou et al., 2011). Intensification of offshore productivity is well-marked by different proxies, such as high opal content, $\delta^{13}C$ difference (planktonic-benthic) and organic carbon content at the same periods (Figs. 5 A-D). It is also supported by the productivity foraminifera-based SIMMAX.28 (Figs. 6B-C-D-E) pointing to rapid and significant environmental changes.

Primary Productivity (Fig. 6D) reflected in Export Production at the open ocean site is different from that at the nearshore sites (Fig. 6B). This disparity illustrates the development of high nutrient levels in coastal zone waters compared to the offshore (oceanic) areas, where its direct influence decreases. Similar records in both sites would imply an influence from terrestrial input or erosion from sea level lowering toward an echo paleoproductivity but with much lower magnitude at the open ocean environment (Thomson et al., 2000). The disparity between the two sites, therefore, sustains productivity originating from the open ocean.

As shown in a more detailed view of the time sequences of events off Iberia over the last climate cycle, cold SST episodes after relatively warm and largely ice-free periods occurred when the predominance changed from northern deep waters (NADW) to southern (AABW) (Martrat et al., 2007). Different origin of bottom waters are likely to be reflected on the surface record, not only on SST but also on productivity as it is suggested by the coeval times of 85 ka and 105 ka productivity-events and GS-22 and GS-24 at Martrat et al. (2007). The similar pattern of the various proxies responding to hydrography and productivity variations is very consistent for the analysed period. Therefore, the harmony of the records reflecting the ocean dynamics and underlying biomass seems to point to a coupling between oceanic productivity and the SOW.

7. Conclusions

Interglacial conditions of MIS5 are compared to glacial stages MIS4 and MIS6 of higher productivity, in areas under the potential influence of a coastal upwelling regime (Pailler and Bard, 2002; Salgueiro et al., 2010). Site MD01-2446 shows higher nutrient supply during Termination II, MIS4, MIS6, and warming transitions of the MIS5 sub-stages. The highest nutrient content (higher productivity) is in phase with tracers of deep-water ventilation variations (benthic $\delta^{13}C$ and $^{231}Pa/^{230}Th$), and therefore establishes evidence of the coupling between productivity variations and the SOW.

The paleoproductivity record explained mainly by the variability of the sub-mesoscale driven vertical nutrient fluxes is in agreement with benthic $\delta^{13}C$ and $^{231}Pa/^{230}Th$. Periods of low benthic $\delta^{13}C$ and high $^{231}Pa/^{230}Th$ (less North Atlantic Deep Water formation, more GNAIW and potentially AAIW and/or mode waters formation) during warming transitions of MIS5 sub-stages which are coeval with higher productivity, suggest a link between oceanic productivity changes and the Atlantic Meridional Overturning Circulation.

If such a link exists, as suggested by the data, it highlights the potential role of the subtropical Atlantic Ocean in the ocean biological carbon pump, over (sub-) glacial-interglacial time scales.

Changes of coarse magnetic grain size in the sediment, combined with enhanced mean carb-free <63 μm and SS%, suggests a distinct source of bottom flow. Coarse magnetic grains are concentrated in silt grain size, and Ti, Fe and K are mainly adsorbed into clays, thus probably recording the long way transport and deposition of sediments during colder periods by the northward SOW current. Both parameters are signs of the dynamics of the bottom current flow and its pathway.

From the Tore Seamount comparison to Iberian nearshore environments [cores MD95-2042 and MD95-2040], a relationship between offshore and overturning circulation is proposed, raising the need of increasing the number of studies on paleoproductivity variations in oligotrophic areas in future research.

Acknowledgements

This research was funded by AMOCINT project (ESF-EUROCORES programme, 06-EuroMARC-FP-008, through FCT EUROMARC/0002/2007).

The British Ocean Sediment Core Repository (BOSCOR) is acknowledged for supplying the sediment samples, through G. Rothwell, and sampling help of L. de Abreu and B. Alker. F. Dewilde is acknowledged for performing the stable oxygen and carbon isotopic analyses and Camille Wandres for helping with the measurements of the magnetic parameters.

Laboratory technical assistance in the LNEG was done by L. Matos (opal), C. Monteiro and D. Ferreira (CHNS) and W. Soares (Sedigraph). R. Mortlock is acknowledged for the support in establishing the methodology for biogenic opal determination at LNEG laboratory and E. Salgueiro for the calculations of Export Production ($gC.m^{-2}.yr^{-1}$) on core D11957. The revision work of two anonymous reviewers and Associate Editor Louisa Irene Bradtmiller greatly improved the quality of the manuscript.

Figure Captions

Figure 1: Location and oceanography

Position of cores MD01-2446 [39.06°N, 12.62°W, 3547 m], D11957P [39.05°N, 12.58°W, 3585 m], MD95-2042 [37.8°N, 10.17°W, 3146 m] and MD95-2040 [40.58°N, 9.86°W, 2465 m].

A) Digital elevation model from (Farr et al., 2007), bathymetry from IOC, IHO and BODC, 2003. Blue dashed arrows indicate the main deep-water mass off Iberian margin, adapted from (van Aken, 2000): Northeast Atlantic Deep Water (NEADW) and the Lower Deep Water (LDW), southern-sourced water mass derived from Antarctic Bottom Water (AABW);

B) Upper ocean winter-time circulation (adapted from (Peliz et al., 2005), where: WIWiF - Western Iberia Winter Front; IPC – Iberian Poleward Current; IPC-A – Alternative path of the Iberian Poleward Current; PC – Portugal Current; GCNR – Gulf of Cadiz Northern Recirculation; RAME – Recurrent Anticyclonic meander/eddy, Swoddies – Slope Water Oceanic Eddies; Meddies – Mediterranean eddies; WIBP – Western Iberia Buoyant Plume.

Figure 2: Surface and deep water masses: offshore (MD01-2446 in red and D11957 in cyan) versus nearshore (MD95-2042 in blue and MD95-2040 in green) of the Iberian margin: A- Planktonic $\delta^{18}O$ (‰) VPDB (*G. bulloides*) from MD01-2446 (this study), MD95-2042 (Cayre et.al. 1999) and MD95-2024 (Abreu etal., 2003); B- SST °C (summer) based on foraminifera Simmax

Transfer Function of cores D11957 (Lebreiro et al., 1997), MD95-2042 (Cayre et al., 1999) and MD95-2040 (Salgueiro et al., 2010); C- Benthic $\delta^{18}O$ (‰) VPDB of cores MD01-2446 (red, this study) and MD95-2042 (blue, Shackleton et al., 2000); D- Benthic $\delta^{13}C$ (‰) VPDB record of cores MD01-2446 (red, this study) and MD95-2042 (blue, Shackleton et al, 2000). Bold lines for each curve indicate 3-point average smoothing.

Figure 3: Core MD01-2446: A- benthic $\delta^{13}C$ record; B- benthic $\delta^{18}O$ record; C- decay corrected excess sedimentary ($^{231}Pa/^{230}Th$) activity ratio (Guihou et al., 2010); bold line indicates 3-point average smoothing; D- paleomagnetic data ARM/IRM, κARM/κ and Mr/Ms (D); E- mean of the carbonate-free <63 μm) is black colour (at right-axis) and SS% (percentage of sortable silt i.e. %(10-63 μm)/<63μm) is grey colour (at left-axis).

Figure 4: A- Relative Sea Level Variation [RSL (m)] from (Waelbroeck et al., 2002); B- $\delta^{18}O$ bulk sediment from core MD01-2446.

Figure 5: Productivity proxies from core MD01-2446: A- Opal content (weight %). Right-side axes are the same parameter ^{230}Th normalized flux (g.cm^{-2}ka^{-1}) (bold line); B- $\delta^{13}C$ difference (*G. bulloides - C. wuellerstorfi*); C- organic carbon (weight %); D- $CaCO_3$ (weight %). Right-side axes are the same parameter ^{230}Th normalized flux (g.cm^{-2}ka^{-1}) (bold line); E- ^{230}Th normalized bulk flux (g.cm^{-2}ka^{-1}) (Guihou et al., 2010); F- Benthic $\delta^{13}C$ record.

Figure 6: Open ocean eddy-pumping versus coastal upwelling productivity.
A- Opal content (weight %) and Opal ^{230}Th normalized flux (g.cm^{-2}ka^{-1}) (thick line) from core MD01-2446; B- Export Production (gC.m^{-2}.yr^{-1}) from core MD95-2042 (thick black line) (Salgueiro et al., 2010) and from core D11957 (grey thin line) (Lebreiro et al., 1997); C- Core D11957 (Lebreiro et al., 1997): Polar, and Gyre Margin (SIMMAX.28 Transfer Function); D- core D11957: Primary Productivity SIMMAX.28; E- Core D11957 (Lebreiro et al., 1997): Upwelling (SIMMAX.28).
Sea Surface Temperatures (SST), Paleoproductivity (PP) and factors FA20 (Polar, Gyre margin, and Upwelling) were estimated through the transfer function SIMMAX28, based on modern analogues (Modern Analogue Technique using a similarity index). For more details see Pflaumann et al. (1996, 2003) and Lebreiro et al. (1997).

Supplementary Figures:

Supplementary Figure 1:

A large phytoplankton bloom off Iberia forming a bluish-green mantle in surface water. Credits from Visible Earth (http://visibleearth.nasa.gov), part of EOS Project Science Office located at NASA Goddard Space Flight Center [Image courtesy Jacques Descloitres, MODIS Land Rapid Response Team at NASA GSFC].

Supplementary Figure 2: Age-depth plot of MD01-2446. Symbols correspond to tie-points of correlation of *G. bulloides* oxygen isotopic records of each core (MD95-2040 and MD01-2446) and the *G. bulloides* oxygen isotopic record of core MD95-2042.

Supplementary Figure 3:

Cross correlation between SS% and “Mean carbonate-free <63 μm fraction” from core MD01-2446.

Supplementary Figure 4:

Relationship between opal (wt%) and $\delta^{13}C$, estimated through the Pearson correlation coefficient r and computed for 152 samples.

Supplementary Figure 5:

Relationship between opal (wt%) and ^{230}Th-normalised opal flux estimated through the Pearson correlation coefficient r and computed for 144 samples.

Supplementary Figure 6:

Sea Surface Temperature distributions off Iberian margin for winter (A- January) and summer (B- July) 2009. Source: POET Data Viewer – AVHRR Pathfinder Version 5 data (http://poet.jpl.nasa.gov).

Supplementary Figure 7:

Sea Surface Temperature (°C) and Salinity (psu) distributions off Iberian margin for spring season (April-June). Figure generated with Ocean Data View (see http://odv.awi.de/).with the World Ocean Atlas 2009 (WOA09).

References

Abrantes, F., 1991. Increased upwelling off Portugal during the last glaciation: Diatom evidence. Marine Micropaleontology 17, 285-310.

Abreu, L.d., Shackleton, N.J., Schönfeld, J., Hall, M., Chapman, M., 2003. Millennial-scale oceanic climate variability of the Western Iberian margin during the last two glacial periods. Marine Geology 196, 1-20.

Adkins, J.F., Ingersoll, A.P., Pasquero, C., 2005. Rapid climate change and conditional instability of the glacial deep ocean from the thermobaric effect and geothermal heating. Quaternary Science Reviews 24, 581-594.

Arístegui, J., Álvarez-Salgado, X.A., Barton, E.D., Figueiras, F.G., Hernández-León, S., Roy, C., Santos, A.M.P., 2004. Oceanography and Fisheries of the Canary current/Iberian region of the Eastern North Atlantic, In: Robinson, A.R., Brink, K.H. (Eds.), The Sea. Harvard University Press, Cambridge, pp. 877-931.

Bazin, L., Landais, A., Lemieux-Dudon, B., Toyé Mahamadou Kele, H., Veres, D., Parrenin, F., Martinerie, P., Ritz, C., Capron, E., Lipenkov, V., Loutre, M.F., Raynaud, D., Vinther, B., Svensson, A., Rasmussen, S.O., Severi, M., Blunier, T., Leuenberger, M., Fischer, H., Masson-Delmotte, V., Chappellaz, J., Wolff, E., 2013. An optimized multi-proxy, multi-site Antarctic ice and gas orbital chronology (AICC2012): 120–800 ka. Clim. Past 9, 1715-1731.

Behrenfeld, M.J., O/'Malley, R.T., Siegel, D.A., McClain, C.R., Sarmiento, J.L., Feldman, G.C., Milligan, A.J., Falkowski, P.G., Letelier, R.M., Boss, E.S., 2006. Climate-driven trends in contemporary ocean productivity. Nature 444, 752-755.

Bianchi, G.G., Hall, I.R., McCave, I.N., Joseph, L., 1999. Measurement of the sortable silt current speed proxy using the Sedigraph 5100 and Coulter Multisizer IIe: precision and accuracy. Sedimentology 46, 1001-1014.

Brachfeld, S., Kissel, C., Laj, C., Mazaud, A., 2004. Viscous behavior of U channels during acquisition and demagnetization of remanences: Implications for paleomagnetic and rock-magnetic investigations. Physics of the Earth and Planetary Interiors 145, doi:10.1016/j.pepi.2003.1012.1011.

Bradtmiller, L.I., McGee, D., Awalt, M., Evers, J., Yerxa, H., Kinsley, C.W., deMenocal, P.B., 2016. Changes in biological productivity along the northwest African margin over the past 20,000 years. Paleoceanography 31, 185-202.

Broecker, W.S., 1982. Glacial to interglacial changes in ocean chemistry. Progress In Oceanography 11, 151-197.

Broecker, W. S. 1982b. Ocean chemistry during glacial time, Geochem. Cosmochim. Acta, 46, 1689–1705.

Cayre, O., Lancelot, Y., Vincent, E., Hall, M.A., 1999. Paleoceanographic reconstructions from planktonic foraminifera off the Iberian Margin: Temperature, salinity, and Heinrich events. Paleoceanography 14, 384-396.

Channell, J.E.T., Hodell, D.A., Margari, V., Skinner, L.C., Tzedakis, P.C., Kesler, M.S., 2013. Biogenic magnetite, detrital hematite, and relative paleointensity in Quaternary sediments from the Southwest Iberian Margin. Earth and Planetary Science Letters 376, 99-109.

Coplen, T.B., 1988. Normalization of oxygen and hydrogen isotope data. Chemical Geology 72, 293–297.

Curry, W.B., Oppo, D.W., 2005. Glacial water mass geometry and the distribution of $\delta^{13}C$ of ΣCO_2 in the western Atlantic Ocean. Paleoceanography 20, doi:10.1029/2004PA001021.

Dufois, F., Hardman-Mountford, N.J., Greenwood, J., Richardson, A.J., Feng, M., Matear, R.J., 2016. Anticyclonic eddies are more productive than cyclonic eddies in subtropical gyres because of winter mixing. Science Advances 2, e1600282.

Eberwein, A., Mackensen, A., 2006. Regional primary productivity differences off Morocco (NW-Africa) recorded by modern benthic foraminifera and their stable carbon isotopic composition. Deep Sea Research Part I: Oceanographic Research Papers 53, 1379-1405.

Emerson, S., Quay, P., Karl, D., Winn, C., Tupas, L., Landry, M., 1997. Experimental determination of the organic carbon flux from open-ocean surface waters. Nature 389, 951-954.

Farr, T.G., Rosen, P.A., Caro, E., Crippen, R., Duren, R., Hensley, S., Kobrick, M., Paller, M., Rodriguez, E., Roth, L., Seal, D., Shaffer, S., Shimada, J., Umland, J., Werner, M., Oskin, M., Burbank, D., Alsdorf, D., 2007. The Shuttle Radar Topography Mission. Reviews of Geophysics 45, RG2004.

Filippelli, G.M., Latimer, J.C., Murray, R.W., Flores, J.-A., 2007. Productivity records from the Southern Ocean and the equatorial Pacific Ocean: Testing the glacial Shelf-Nutrient Hypothesis. Deep Sea Research Part II: Topical Studies in Oceanography 54, 2443-2452.

Fiúza, A.F.G., 1983. Upwelling patterns off Portugal, In: Suess, E., Thiede, J. (Ed.), Coastal Upwelling Its Sediment Record. Plenum Press, New York, pp. 85–98.

Fiúza, A.F.G., 1984. Hidrologia e Dinamica das Aguas Costeiras de Portugal, Faculdade de Ciências da Universidade de Lisboa. Universidade de Lisboa, Lisboa, p. 294.

François, R., Frank, M., van der Loeff, M.M.R., Bacon, M.P., 2004. ^{230}Th normalization: An essential tool for interpreting sedimentary fluxes during the late Quaternary. Paleoceanography 19, PA1018, doi:1010.1029/2003PA000939.

Gil, I.M., Keigwin, L.D., Abrantes, F.G., 2009. Deglacial diatom productivity and surface ocean properties over the Bermuda Rise, northeast Sargasso Sea. Paleoceanography 24.

Govin, A., Chiessi, C.M., Zabel, M., Sawakuchi, A.O., Heslop, D., Hörner, T., Zhang, Y., Mulitza, S., 2014. Terrigenous input off northern South America driven by changes in Amazonian climate and the North Brazil Current retroflection during the last 250 ka. Climate of the Past 10, 843-862.

Guihou, A., Pichat, S., Govin, A., Nave, S., Michel, E., Duplessy, J.-C., Telouk, P., Labeyrie, L., 2011. Enhanced Atlantic Meridional Overturning Circulation supports the Last Glacial Inception. Quaternary Science Reviews 30, 1576-1582.

Guihou, A., Pichat, S., Nave, S., Govin, A., Labeyrie, L., Michel, E., Waelbroeck, C., 2010. Late slowdown of the Atlantic Meridional Overturning Circulation during the Last Glacial Inception: New constraints from sedimentary (231Pa/230Th). Earth and Planetary Science Letters 289, 520-529.

Hall, I.R., McCave, I.N., 2000. Palaeocurrent reconstruction, sediment and thorium focussing on the Iberian margin over the last 140 ka. Earth and Planetary Science Letters 178, 151-164.

Hendry, K.R., Gong, X., Knorr, G., Pike, J., Hall, I.R., 2016. Deglacial diatom production in the tropical North Atlantic driven by enhanced silicic acid supply. Earth and Planetary Science Letters 438, 122-129.

Incarbona, A., Martrat, B., Stefano, E.D., Grimalt, J.O., Pelosi, N., Patti, B., Tranchida, G., 2010. Primary productivity variability on the Atlantic Iberian Margin over the last 70,000 years: Evidence from coccolithophores and fossil organic compounds. Paleoceanography 25, PA2218.

Jennings, S., Kaiser, M.J., Reynolds, J.D., 2001. Marine Fisheries Ecology. Blackwell, Oxford.

King, G.C.P., Banerjee, S.K., Marvin, J., Özdemir, Ö., 1982. A comparison of different magnetic methods for determining the relative grain size of magnetite in natural materials: Some results from lake sediments. Earth and Planetary Science Letters 59, 404-419.

Kissel, C., 2005. Magnetic signature of rapid climatic variations in glacial North Atlantic, a review. Comptes Rendus Geosciences 337, 908-918.

Kukla, G.J., Bender, M.L., Beaulieu, J.-L.d., Bond, G., Broecker, W.S., Cleveringa, P., Gavin, J.E., Herbert, T.D., Imbrie, J., Jouzel, J., Keigwin, L.D., Knudsen, K.-L., McManus, J.F., Merkt, J., Muhs, D.R., Müller, H., Poore, R.Z., Porter, S.C., Seret, G., Shackleton, N.J., Turner, C., Tzedakis, P.C., Winograd, I.J., 2002. Last Interglacial Climates. Quaternary Research 58, 2–13.

Lebreiro, S.M., Francés, G., Abrantes, F.F.G., Diz, P., Bartels-Jónsdóttir, H.B., Stroynowski, Z.N., Gil, I.M., Pena, L.D., Rodrigues, T., Jones, P.D., Nombela, M.A., Alejo, I., Briffa, K.R., Harris, I., Grimalt, J.O., 2006. Climate change and coastal hydrographic response along the Atlantic Iberian margin (Tagus Prodelta and Muros Ría) during the last two millennia. The Holocene 16, 1003-1015.

Lebreiro, S.M., Moreno, J.C., Abrantes, F.F., Pflaumann, U., 1997. Productivity and paleoceanographic implications on the Tore Seamount (Iberian Margin) during the last 225 Kyr: Foraminiferal evidence. Paleoceanography 12, 718-727.

Lebreiro, S.M., Voelker, A.H.L., Vizcaino, A., Abrantes, F.G., Alt-Epping, U., Jung, S., Thouveny, N., Gràcia, E., 2009. Sediment instability on the Portuguese continental margin under abrupt glacial climate changes (last 60 kyr). Quaternary Science Reviews 28, 3211-3223.

Lévy, M., 2003. Mesoscale variability of phytoplankton and of new production: Impact of the large-scale nutrient distribution. Journal of Geophysical Research 108, doi:10.1029/2002JC001577.

Lisiecki, L.E., Raymo, M.E., 2005. A Pliocene-Pleistocene stack of 57 globally distributed benthic $\delta^{18}O$ records. Paleoceanography 20, PA1003, doi:1010.1029/2004PA001071.

Lombard, F., Labeyrie, L., Michel, E., Bopp, L., Cortijo, E., Retailleau, S., Howa, H., Jorissen, F., 2011. Modelling planktic foraminifer growth and distribution using an ecophysiological multi-species approach. Biogeosciences 8, 853-873.

Martins, Maria Virgínia Alves; Rey, Daniel; Pereira, Egberto; Plaza-Morlote, Maider; Salgueiro, Emília; Moreno, João; Duleba, Wânia; Ribeiro, Sara; dos Santos, José Francisco; Bernabeu, Ana; Rubio, Belén; Laut, Lazaro Luiz Mattos; Frontalini, Fabrizio; da Conceição Rodrigues, Maria Antonieta; Rocha, Fernando , 2017: Influence of dominant wind patterns in a distal region of the NW Iberian Margin during the last glaciation. Geological Society of London.

Marino, M., Maiorano, P., Tarantino, F., Voelker, A., Capotondi, L., Girone, A., Lirer, F., Flores, J.-A., Naafs, B.D.A., 2014. Coccolithophores as proxy of seawater changes at orbital-to-millennial scale during middle Pleistocene Marine Isotope Stages 14–9 in North Atlantic core MD01-2446. Paleoceanography 29, 2013PA002574.

Martrat, B., Grimalt, J.O., Shackleton, N.J., de Abreu, L., Hutterli, M.A., Stocker, T.F., 2007. Four Climate Cycles of Recurring Deep and Surface Water Destabilizations on the Iberian Margin. Science 317, 502-507.

McCave, I.N., Manighetti, B., Robinson, S.G., 1995. Sortable silt and fine sediment size/composition slicing: Parameters for palaeocurrent speed and palaeoceanography. Paleoceanography 10, 593-610.

McCave, I.N., Hall, I.R., 2006. Size sorting in marine muds: Processes, pitfalls, and prospects for paleoflow-speed proxies. Geochemistry, Geophysics, Geosystems 7, Q10N05.

McCave, I.N., Thornalley, D.J.R., Hall, I.R., 2017. Relation of sortable silt grain-size to deep-sea current speeds: Calibration of the 'Mud Current Meter'. Deep Sea Research Part I: Oceanographic Research Papers 127, 1-12.

McGillicuddy, D.J., Anderson, L.A., Bates, N.R., Bibby, T., Buesseler, K.O., Carlson, C.A., Davis, C.S., Ewart, C., Falkowski, P.G., Goldthwait, S.A., Hansell, D.A., Jenkins, W.J., Johnson, R., Kosnyrev, V.K., Ledwell, J.R., Li, Q.P., Siegel, D.A., Steinberg, D.K., 2007. Eddy/Wind Interactions Stimulate Extraordinary Mid-Ocean Plankton Blooms. Science 316, 1021-1026.

McGillicuddy, D.J., Robinson, A.R., Siegel, D.A., Jannasch, H.W., Johnson, R., Dickey, T.D., McNeil, J., Michaels, A.F., Knap, A.H., 1998. Influence of mesoscale eddies on new production in the Sargasso Sea. Nature 394, 263-266.

Meckler, A.N., et al., 2013. Deglacial pulses of deep-ocean silicate into the subtropical North Atlantic Ocean. Nature 495 (7442), 495–498.

Michel, E., Labeyrie, L.D., Duplessy, J.-C., Gorfti, N., Labracherie, M., Turon, J.-L., 1995. Could Deep Subantarctic Convection Feed the World Deep Basins during the Last Glacial Maximum? Paleoceanography 10, 927-941.

Mortlock, R.A., Froelich, P., 1989. A simple method for the rapid determination of biogenic opal in pelagic marine sediments. Deep-Sea Research 36, 1415-1426.

Nave, S., Freitas, P., Abrantes, F., 2001. Coastal upwelling in the Canary Island region: spatial variability reflected by the surface sediment diatom record. Marine Micropaleontology 42, 1-23.

Oliveira, P.B., Peliz, A., Dubert, J., Rosa, T.L., Santos, A.M.P., 2004. Winter geostrophic currents and eddies in the western Iberia coastal transition zone. Deep Sea Research Part I: Oceanographic Research Papers 51, 367-381.

Oliver, K.I.C., Hoogakker, B.A.A., Crowhurst, S., Henderson, G.M., Rickaby, R.E.M., Edwards, N.R., Elderfield, H., 2010. A synthesis of marine sediment core δ13C data over the last 150 000 years. Clim. Past J1 - CP 6, 645-673.

Oschlies, A., 2002. Can eddies make ocean deserts bloom? Global Biogeochemical Cycles 16, 1106.

Oschlies, A., Garcon, V., 1998. Eddy-induced enhancement of primary production in a model of the North Atlantic Ocean. Nature 394, 266-269.

Pahnke, K., Goldstein, S.L., Hemming, S.R., 2008. Abrupt changes in Antarctic Intermediate Water circulation over the past 25,000 years. Nature Geoscience 1, 870-874.

Paillard, D., Labeyrie, L., Yiou, P., 1996. Macintosh program performs time-series analysis. Eos Trans. AGU 77, 379.

Pailler, D., Bard, E., 2002. High frequency palaeoceanographic changes during the past 140 000 yr recorded by the organic matter in sediments of the Iberian Margin. Palaeogeography, Palaeoclimatology, Palaeoecology 181, 431-452.

Pelegri, J.L., Aristegui, J., Cana, L., Gonzalez-Davila, M., Hernandez-Guerra, A., Hernandez-Leon, S., Marrero-Diaz, A., Montero, M.F., Sangra, P., Santana-Casiano, M., 2005. Coupling between the open ocean and the coastal upwelling region off northwest Africa: water recirculation and offshore pumping of organic matter. Journal of Marine Systems 54, 3-37.

Peliz, A., Dubert, J., Santos, A.M.P., Oliveira, P.B., Cann, B.L., 2005. Winter upper ocean circulation in the Western Iberian Basin--Fronts, Eddies and Poleward Flows: an overview. Deep Sea Research Part I: Oceanographic Research Papers 52, 621-646.

Pflaumann, U., Duprat, J., Pujol, C., Labeyrie, L.D., 1996. SIMMAX: A modern analog technique to deduce Atlantic sea surface temperatures from planktonic foraminifera in deep-sea sediments. Paleoceanography 11, 15-35.

Pflaumann, U., Sarnthein, M., Chapman, M., d'Abreu, L., Funnell, B., Huels, M., Kiefer, T., Maslin, M., Schulz, H., Swallow, J., Kreveld, S.v., Vautravers, M., Vogelsang, E., Weinelt, M., 2003. Glacial North Atlantic: Sea-surface conditions reconstructed by GLAMAP 2000. Paleoceanography 18, 1065, doi:1010.1029/2002PA000774.

Rickaby, R.E.M., Elderfield, H., 2005. Evidence from the high-latitude North Atlantic for variations in Antarctic Intermediate water flow during the last deglaciation. Geochemistry, Geophysics, Geosystems 6, n/a-n/a.

Romero, O.E., Kim, J.-H., Donner, B., 2008. Submillennial-to-millennial variability of diatom production off Mauritania, NW Africa, during the last glacial cycle. Paleoceanography 23.

Shackleton, Nicholas J; Hall, Michael A; Vincent, Edith (2000): Phase relationships between millennial-scale events 64,000-24,000 years ago. Paleoceanography, 15(6), 565-569, doi:10.1029/2000PA000513

Salgueiro, E., Voelker, A.H.L., Abreu, L.d., Abrantes, F., Meggers, H., Wefer, G., 2010. Temperature and productivity changes off the western Iberian margin during the last 150 ky. Quaternary Science Reviews 29, 680-695.

Sanchez Goni, M.F., Loutre, M.F., Crucifix, M., Peyron, O., Santos, L., Duprat, J., Malaize, B., Turon, J.-L., Peypouquet, J.-P., 2005. Increasing vegetation and climate gradient in Western Europe over the Last Glacial Inception (122-110 ka): data-model comparison. Earth and Planetary Science Letters 231, 111-130.

Sarmiento, J.L. and Gruber, N., 2002. Sinks for anthropogenic carbon. Physics today 55 (8), 30-36.

Schmieder, F., Dobeneck, T.v., Bleil, U., 2000. The Mid-Pleistocene climate transition as documented in the deep South Atlantic Ocean: initiation, interim state and terminal event. Earth and Planetary Science Letters 179, 539-549.

Schmittner, A., 2005. Decline of the marine ecosystem caused by a reduction in the Atlantic overturning circulation. Nature 434, 628-633.

Schwab, C., Kinkel, H., Weinelt, M., Repschläger, J., 2012. Coccolithophore paleoproductivity and ecology response to deglacial and Holocene changes in the Azores Current System. Paleoceanography 27, PA3210.

Shackleton, N.J., Hall, M.A., Vincent, E., 2000. Phase relationships between millennial-scale events 64 000 - 24 000 years ago. Paleoceanography 15, 565-569.

Shackleton, N. J., Hall, M. A., Line, J., and Cang, S., 1983. Carbon isotope data in core V19-30 confirm reduced carbon dioxide concentration in the ice age atmosphere, Nature, 306, 319–322.

Shackleton, N.J., Opdyke, N.D., 1973. Oxygen isotope and palaeomagnetic stratigraphy of Equatorial Pacific core V28-238: Oxygen isotope temperatures and ice volumes on a 105 year and 106 year scale. Quaternary Research 3, 39-55.

Sousa, F.M., Bricaud, A., 1992. Satellite-Derived Phytoplankton Pigment Structures in the Portuguese Upwelling Area. Journal of Geophysical Research 97, 11343-11356.

Stein, R., 1990. Organic Carbon Content/Sedimentation Rate Relationship and its Paleoenvironmental Significance for Marine Sediments. Geo-Marine Letters 10, 37-44.

Thomson, J., Nixon, S., Summerhayes, C.P., Rohling, E.J., Schönfeld, J., Zahn, R., Zahn, P., Abrantes, F.G., Gaspar, L., Vaqueiro, S., 2000. Enhanced productivity on the Iberian margin during glacial/interglacial transitions revealed by barium and diatoms. Journal of the Geological Society, London 157, 667-677.

van Aken, H.M., 2000. The hydrography of the mid-latitude northeast Atlantic Ocean: I: The deep water masses. Deep Sea Research Part I: Oceanographic Research Papers 47, 757-788.

Veres, D., Bazin, L., Landais, A., Toyé Mahamadou Kele, H., Lemieux-Dudon, B., Parrenin, F., Martinerie, P., Blayo, E., Blunier, T., Capron, E., Chappellaz, J., Rasmussen, S.O., Severi, M., Svensson, A., Vinther, B., Wolff, E.W., 2013. The Antarctic ice core chronology (AICC2012): an optimized multi-parameter and multi-site dating approach for the last 120 thousand years. Climate of the Past 9, 1733-1748.

Waelbroeck, C., Labeyrie, L., Michel, E., Duplessy, J.C., McManus, J.F., Lambeck, K., Balbon, E., Labracherie, M., 2002. Sea-level and deep water temperature changes derived from benthic foraminifera isotopic records. Quaternary Science Reviews 21, 295 –305.

Waelbroeck, C., Skinner, L.C., Labeyrie, L., Duplessy, J.C., Michel, E., Vazquez Riveiros, N., Gherardi, J.M., Dewilde, F., 2011. The timing of deglacial circulation changes in the Atlantic. Paleoceanography 26, PA3213.

Weeks, R., Laj, C., Endignoux, L., Fuller, M., Roberts, A., Manganne, R., Blanchard, E., Goree, W., 1993. Improvements in long-core measurement techniques: Applications in palaeomagnetism and palaeoceanography. Geophysical Journal International 114, 651–662, doi:610.1111/j.1365-1246X.1993.tb06994.x.

Williams, R.G., 2011. Ocean eddies and plankton blooms. Nature Geosciences 4, 739-740.

Williams, R.G., Follows, M.J., 1998. Eddies make ocean deserts bloom. Nature 394, 228-229.

Yamazaki, T., Ikehara, M., 2012. Origin of magnetic mineral concentration variation in the Southern Ocean. Paleoceanography 27, PA2206.

Figure 1

Click here to download Figure Fig_1.tif

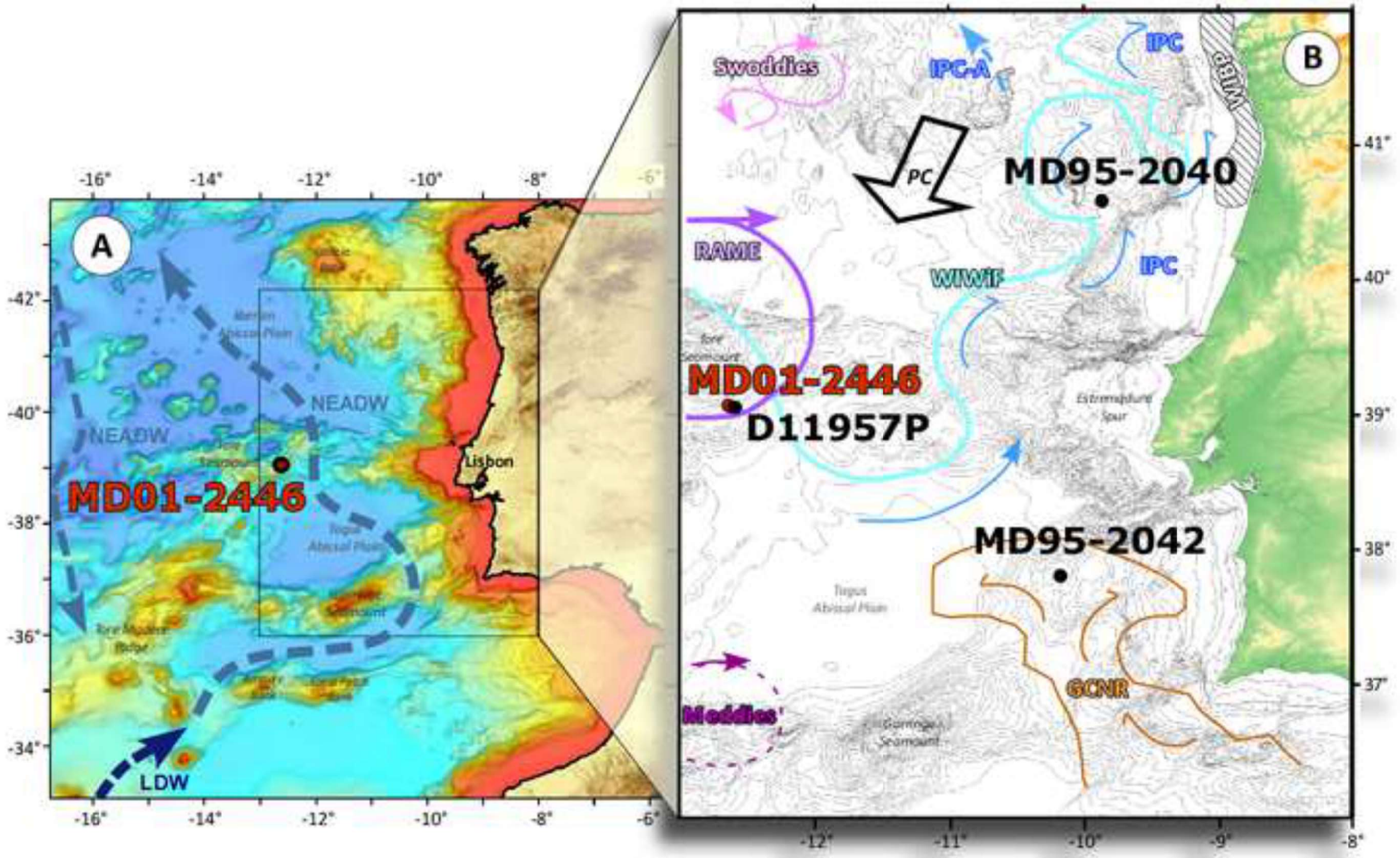

Figure 2

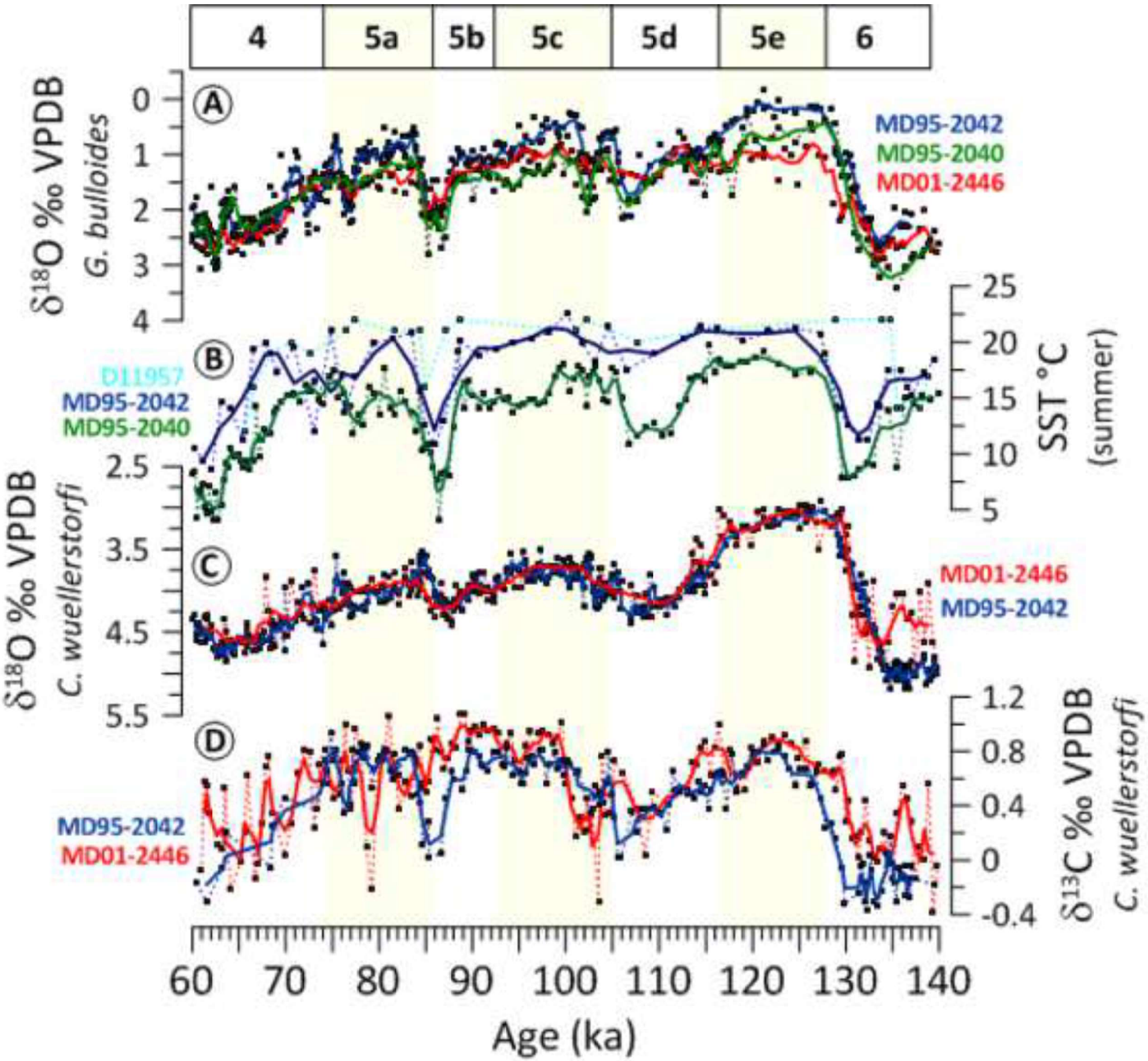
4
5a
5b
5c
5d
5e
6
A
B
C
D
δ18O ‰ VPDB
G. bulloides
MD95-2042
MD95-2040
MD01-2446
D11957
SST °C
(summer)
C. wuellerstorfi
δ13C ‰ VPDB
Age (ka)

Figure 3

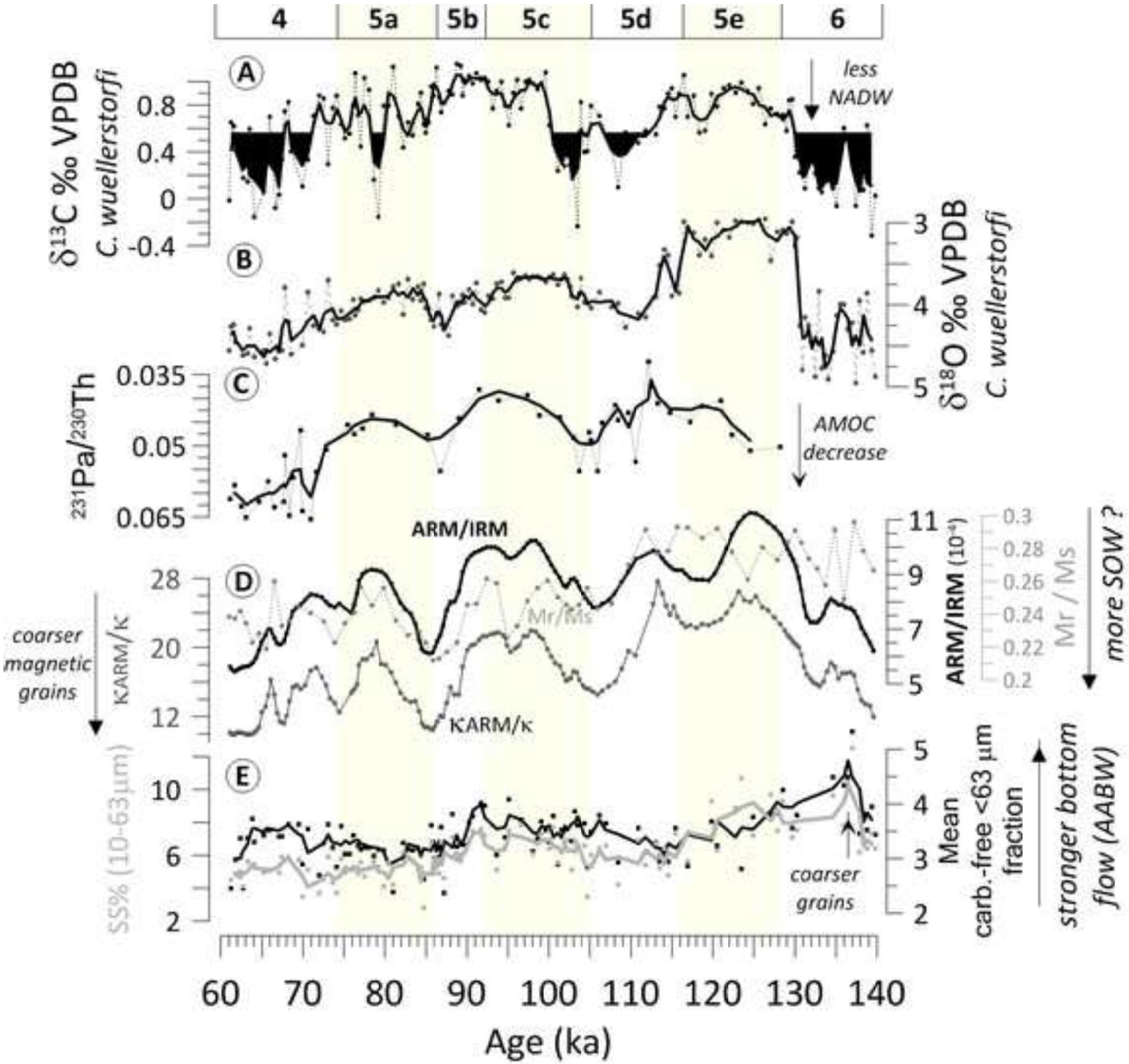
4
5a
5b
5c
5d
5e
6
A
B
C
D
E
less NADW
AMOC decrease
δ13C ‰ VPDB
C. wuellerstorfi
0.8
0.4
0
-0.4
δ18O ‰ VPDB
C. wuellerstorfi
3
4
5
231Pa/230Th
0.035
0.05
0.065
ARM/IRM
Mr/Ms
κARM/κ
coarser magnetic grains
28
20
12
11
9
7
5
ARM/IRM (10-4)
0.3
0.28
0.26
0.24
0.22
0.2
Mr / Ms
more SOW ?
SS% (10-63µm)
10
6
2
Mean carb.-free <63 µm fraction
4
3
coarser grains
stronger bottom flow (AABW)
60
70
80
90
100
110
120
130
140
Age (ka)

Figure 4

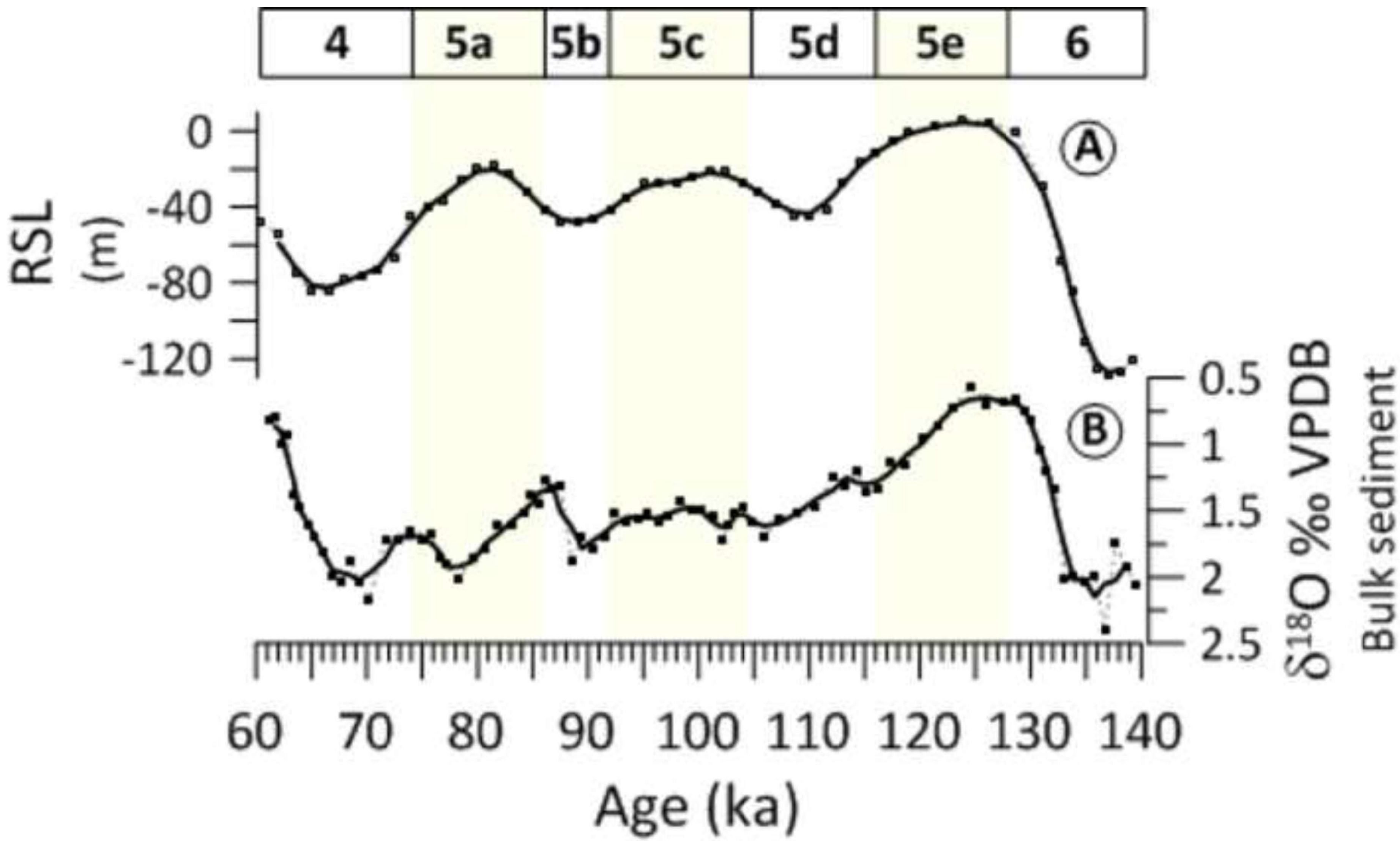

4
5a
5b
5c
5d
5e
6
A
B
RSL (m)
0
-40
-80
-120
0.5
1
1.5
2
2.5
δ18O ‰ VPDB
Bulk sediment
60
70
80
90
100
110
120
130
140
Age (ka)

Figure 5

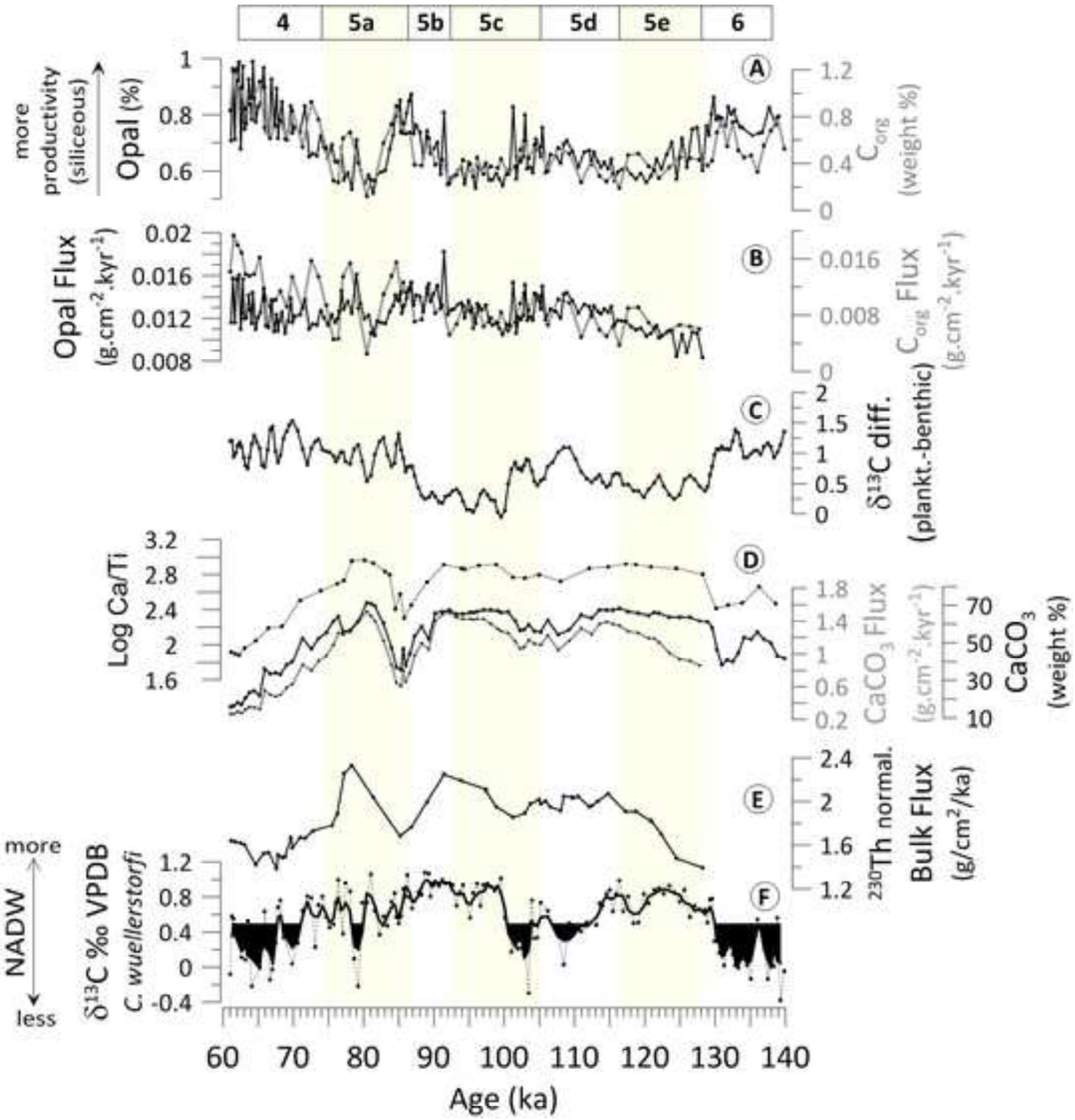
4
5a
5b
5c
5d
5e
6
A
B
C
D
E
F
more productivity (siliceous)
Opal (%)
C_{org} (weight %)
Opal Flux (g.cm^{-2}.kyr^{-1})
C_{org} Flux (g.cm^{-2}.kyr^{-1})
δ^{13}C diff. (plankt.-benthic)
Log Ca/Ti
$CaCO_3$ Flux (g.cm^{-2}.kyr^{-1})
$CaCO_3$ (weight %)
^{230}Th normal. Bulk Flux (g/cm^2/ka)
more
NADW
less
δ^{13}C ‰ VPDB
C. wuellerstorfi
Age (ka)

Figure 6

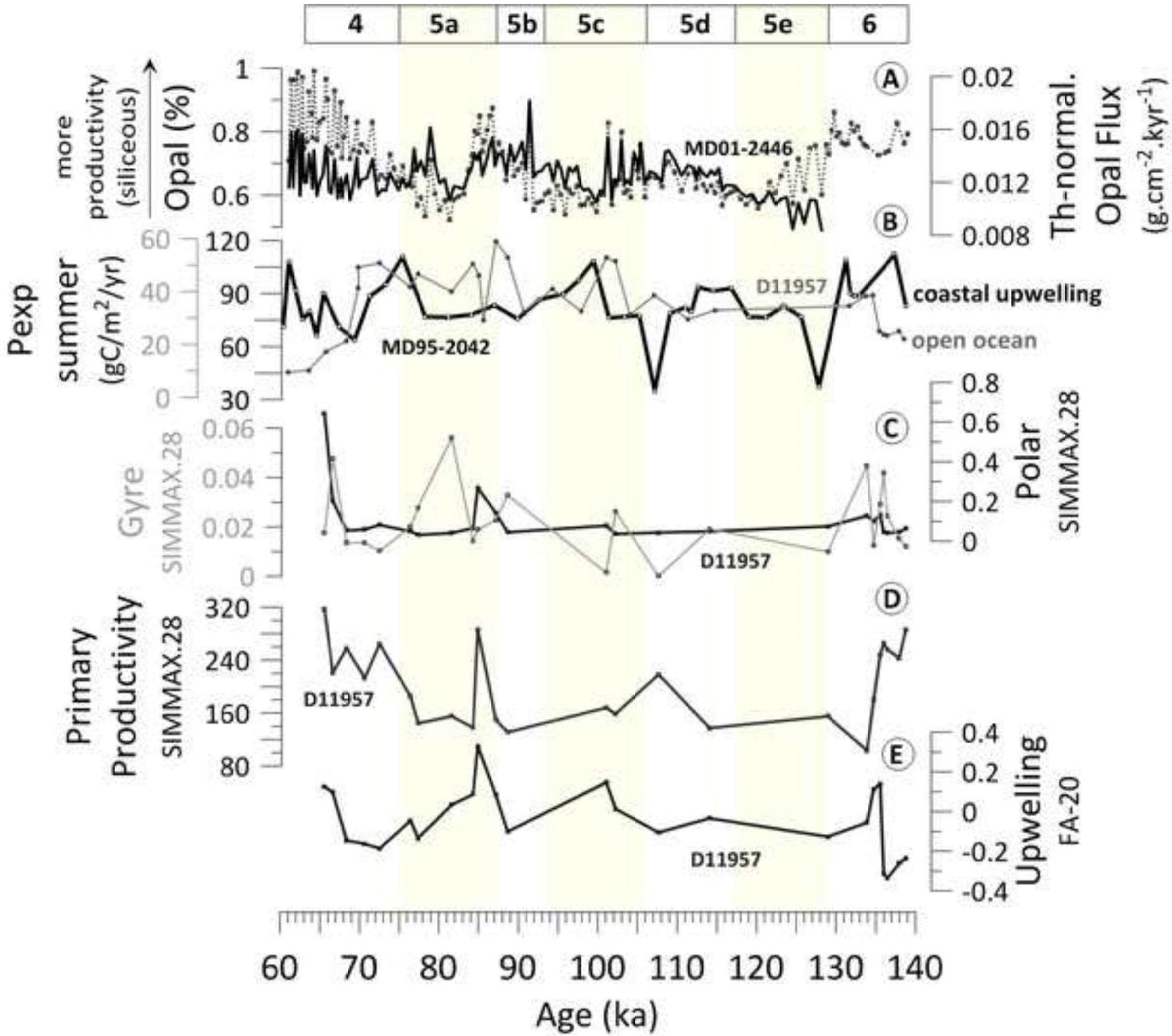
4
5a
5b
5c
5d
5e
6
more productivity (siliceous)
Opal (%)
1
0.8
0.6
A
0.02
0.016
0.012
0.008
Th-normal. Opal Flux (g.cm-2.kyr-1)
MD01-2446
B
Pexp summer (gC/m2/yr)
60
40
20
0
120
90
60
30
D11957
coastal upwelling
open ocean
MD95-2042
C
Gyre SIMMAX.28
0.06
0.04
0.02
0
0.8
0.6
0.4
0.2
0
Polar SIMMAX.28
D11957
D
Primary Productivity SIMMAX.28
320
240
160
80
D11957
E
0.4
0.2
0
-0.2
-0.4
Upwelling FA-20
D11957
60
70
80
90
100
110
120
130
140
Age (ka)

Supplemental Fig1

Click here to download Supplemental Material (Online Only) Spp-Fig1.tif

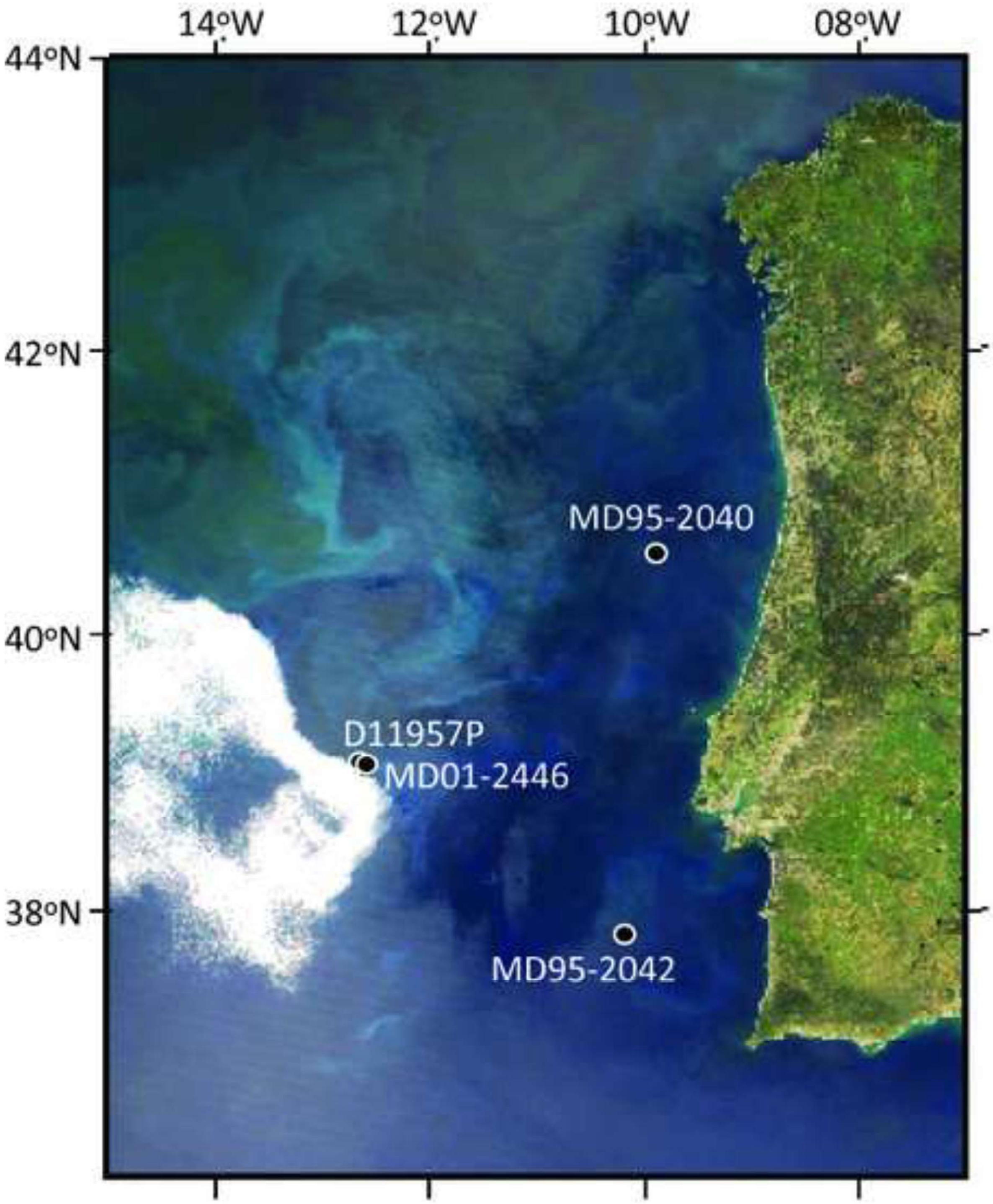

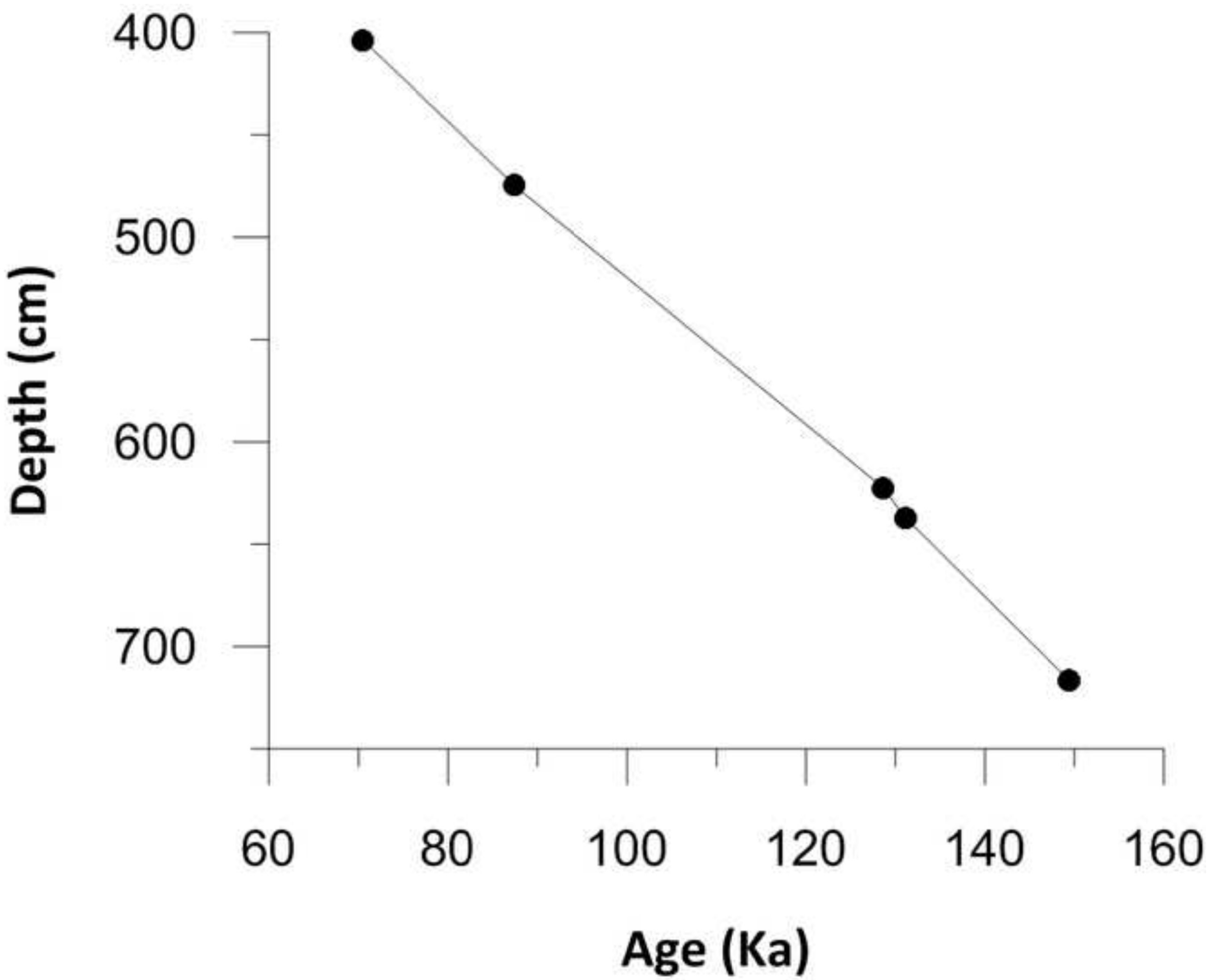
400
500
600
700
Depth (cm)
60
80
100
120
140
160
Age (Ka)

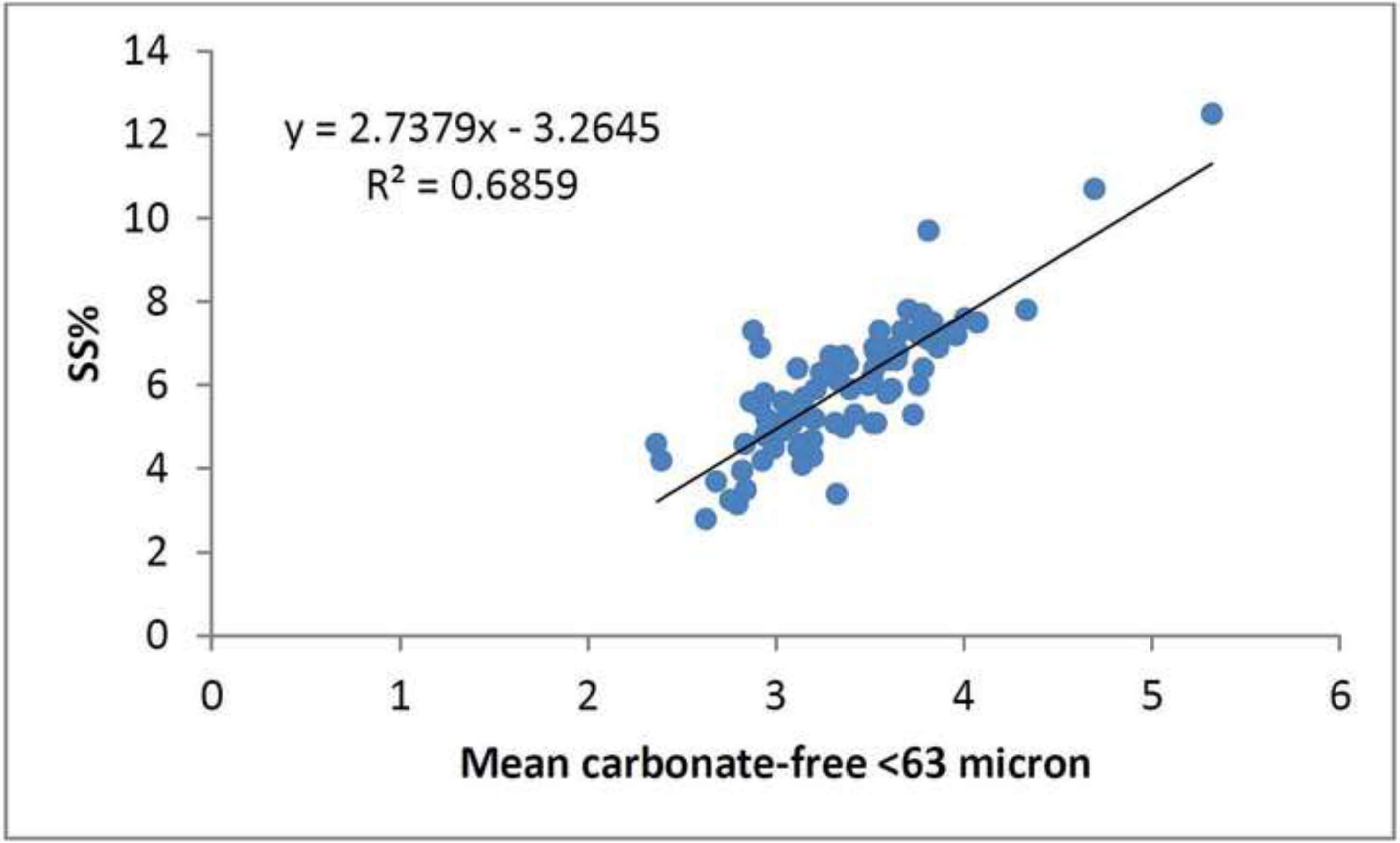
y = 2.7379x - 3.2645
R² = 0.6859
SS%
0
2
4
6
8
10
12
14
0
1
2
3
4
5
6
Mean carbonate-free <63 micron

Supplemental Fig4

Click here to download Supplemental Material (Online Only) Spp-Fig4.png

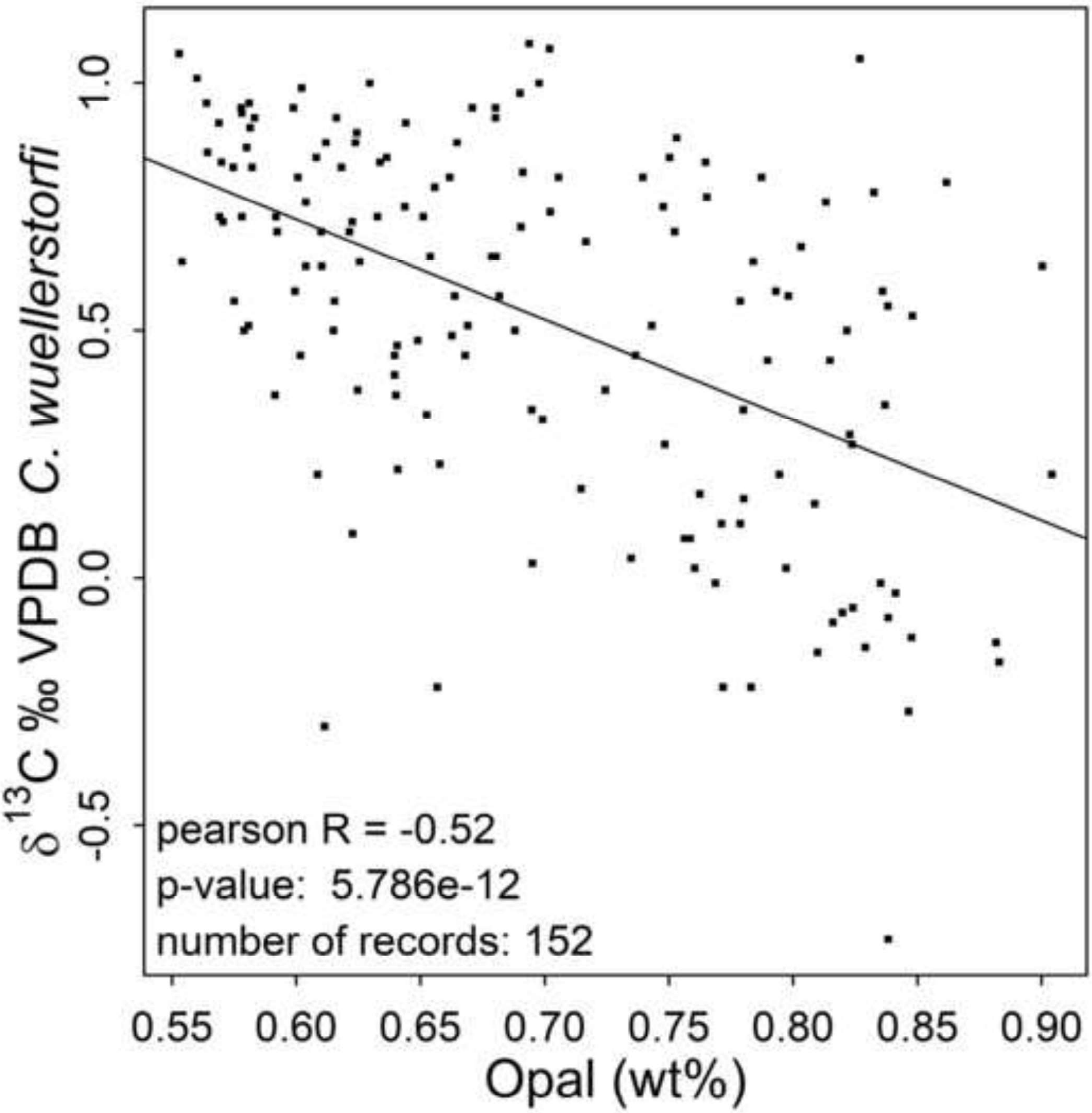

Supplemental Fig5

Click here to download Supplemental Material (Online Only) Spp-Fig5.png

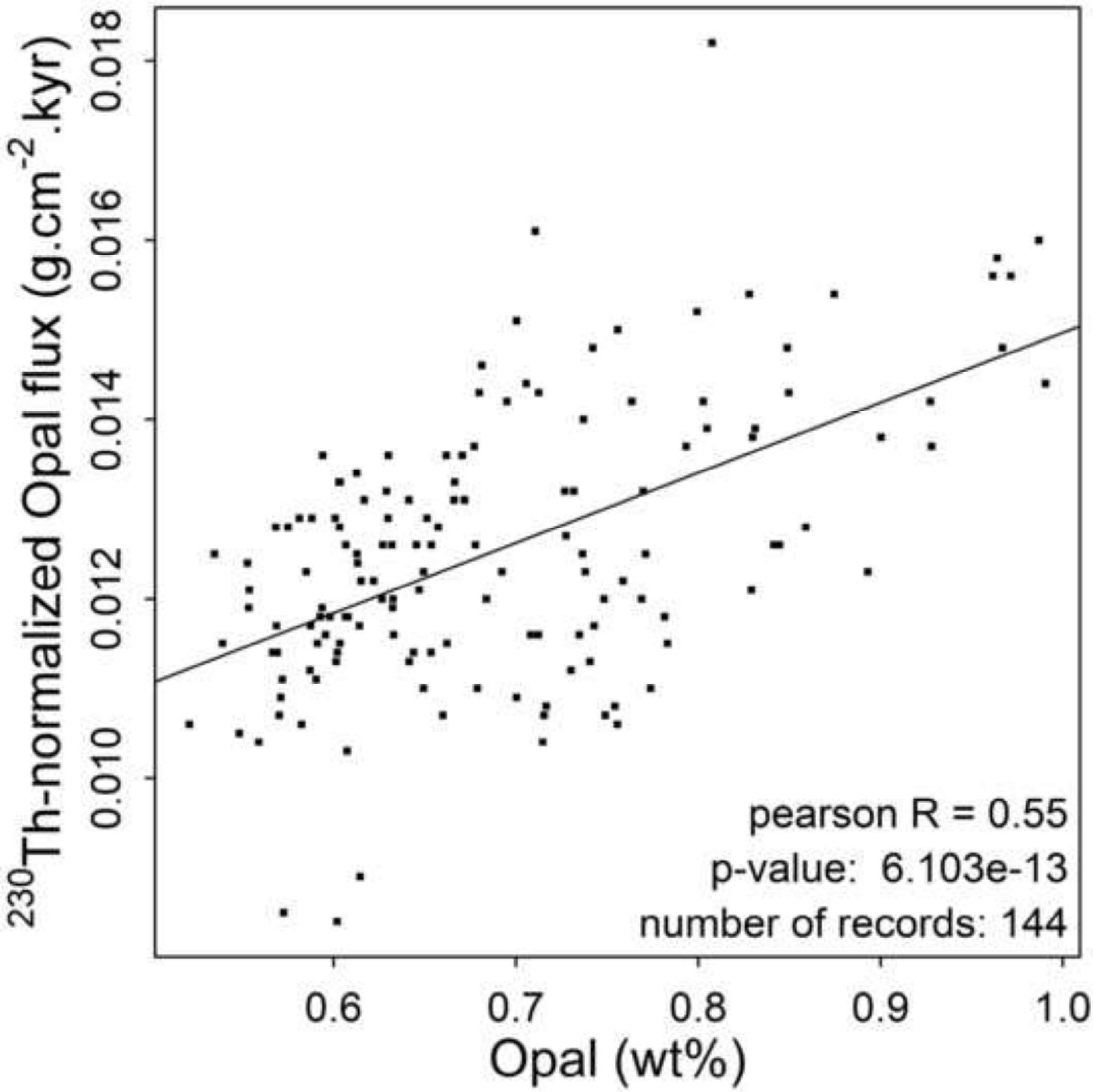

Supplemental Fig6

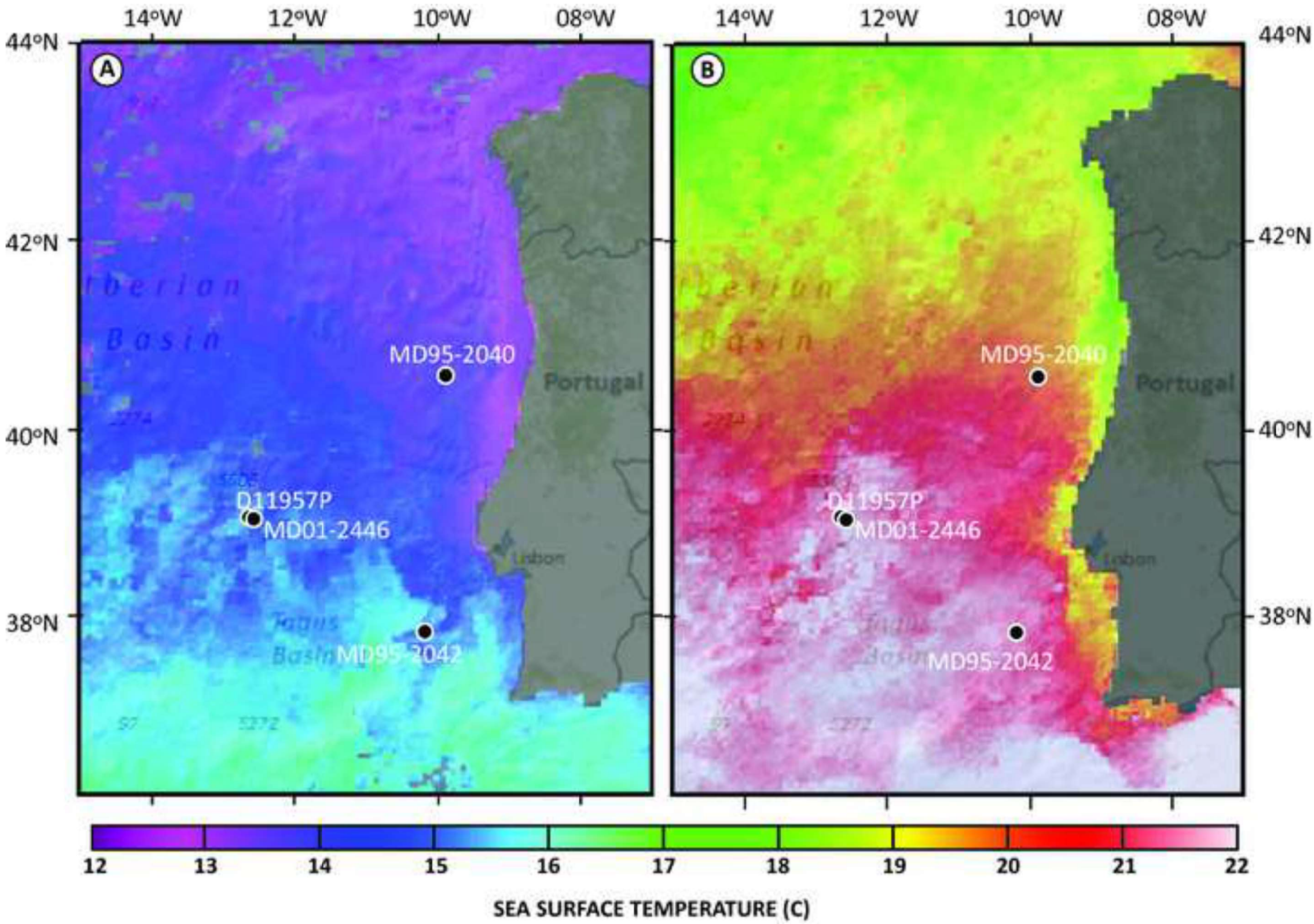

Supplemental Fig7